Eindhoven University of Technology

BACHELOR

Time integration methods for gradient-index media using Hamiltonian Optics

Menting, Kevin

Award date:
2021

Link to publication

Disclaimer
This document contains a student thesis (bachelor's or master's), as authored by a student at Eindhoven University of Technology. Student theses are made available in the TU/e repository upon obtaining the required degree. The grade received is not published on the document as presented in the repository. The required complexity or quality of research of student theses may vary by program, and the required minimum study period may vary in duration.

General rights
Copyright and moral rights for the publications made accessible in the public portal are retained by the authors and/or other copyright owners and it is a condition of accessing publications that users recognise and abide by the legal requirements associated with these rights.

- Users may download and print one copy of any publication from the public portal for the purpose of private study or research.
- You may not further distribute the material or use it for any profit-making activity or commercial gain

Time integration methods for gradient-index media using Hamiltonian Optics

Kevin T. W. Menting

Supervisor:
Jan H. M. ten Thije Boonkkamp

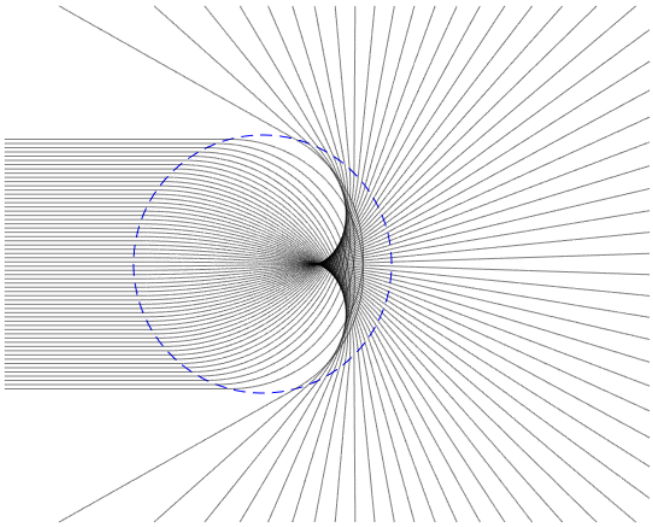

EINDHOVEN UNIVERSITY OF TECHNOLOGY

Department of Mathematics and Computer Science
Eindhoven University of Technology
The Netherlands
11th February 2021

Abstract

In this report, the propagation of light is simulated through various gradient-index lenses. This is done under the assumptions of the Geometric Optics model, which considers light as *rays* and *wavefronts*. In the report, the *eikonal equation*, describing wavefronts, will be characterised by a system of ordinary differential equations (ODEs). Together with initial conditions, we are able to find a solution to this system of ODEs. More interestingly, the solution of this system is in fact a light ray. We can approximate the solution by means of a time integration method. The report covers basic Euler methods, symplectic Euler methods, a Runge-Kutta method and a Gauss-Legendre method. The Luneburg lens, Maxwell's fish-eye lens and a gradient-index lens with cylindrical symmetry will be used to verify the simulation of rays and wavefronts. The report also describes in detail how the system of ODEs can be written as a separable Hamiltonian system. This enables the use of symplectic methods. We will see that within this report, the rays and wavefronts are best approximated by the fourth-order Gauss-Legendre method.

Contents

Introduction

The behavior of light is something which has intrigued mankind for centuries. The study of this is referred to as *Optics*. The theory of light as we know today, has been established over a huge time period by critical thinkers all around the globe. The first theories go back to the classical period of ancient Greece. One of these theories on the nature of light was the extramission theory of light, backed by the famous Greek philosopher Plato (428 B.C. - 328 B.C.). In this theory, light was said to be emitted by our eyes, making us perceive objects [1]. In the same period, the Greek mathematician Euclid of Alexandria (300 B.C.) introduced important geometrical concepts that described the effects of vision, without defining the nature of light [1]. He laid the foundation for what is called *Geometric optics*. More than a millennium passed before Alhazan (965-1040) proved the extramission theory to be wrong [1]. Centuries later, during the Scientific Revolution in Europe, Sir Isaac Newton (1642-1727) contributed to the theory of light. He was one of the scientists that supported the corpuscular theory of light, which states that light is made up of small discrete particles. However, there were also contemporaries, like Christiaan Huygens (1629-1695), who suggested a wave picture of light [1]. Although the particle theory of light remained popular for a long time, Thomas Young (1773-1829) demonstrated in 1802 the wave nature of light through his famous *double-slit experiment* [1]. After that, thinkers like Albert Einstein (1879-1955) and the birth of quantum mechanics, again, drastically changed our way of thinking about light.

Two concepts that are well understood because of optics are the lens and laser. Both concepts are fundamental for a lot of inventions of the past decades. We can study the behaviour of light in a lens or laser without beforehand having to make the actual lens. This is because we understand the nature of light so well. In this report we will try to describe this nature of light from optics in a mathematical perspective. In particular, we will focus on studying the path light takes. This continuous path, with a starting point and ending point, is what we define to be a *ray*. We will focus on the branch of optics called *Geometric optics* or *Ray optics*. Geometric optics is a simplified model for light propagation. The model is restricted in the sense that it does not take into account the wave nature of light [2], which means that optical effects like diffraction and interference are not taken into account. It simplifies the nature of light by considering the propagation as straight lines that bend when the refractive index of the medium changes. Geometric optics works well as an approximation when the wavelength of the light is small compared to the dimensions of the bodies it interacts with. Figure 1 shows a simple example where the Geometric optics model works perfectly. Light is represented as straight lines that refract at the edge of the prism, creating straight lines for each colour.

Figure 1: Album cover of *The Dark Side Of The Moon* by Pink Floyd.

In the first half of the report, we will be concerned with formulating the mathematical objects representing light in the Geometric optics model. In particular, in Chapter 1, light will be represented by rays and wavefronts, using the so-called *eikonal equation*. Wavefronts are surfaces perpendicular to rays. This eikonal equation can be characterised by a system of ordinary differential equations. This is done by the use of the *method of characteristics*. Together with initial conditions, the solution of the ODE system can be found and represents a single ray. In the second half of Chapter 1, wavefronts and rays will be described in terms of polar coordinates. In Chapter 2, the ODE system will be written as a Hamiltonian system. In order to simulate rays, we need to solve the ODE systems of Chapter 1 and 2. Analytical solutions are often hard to find, therefore numerical methods are useful. In Chapter 3 various time integration methods are discussed that can be used to simulate rays. In Chapter 4, various *gradient-index* lenses are introduced to verify the model. In Chapter 5, numerical results are given together with an error comparison of the various numerical methods. Finally, we like to make some recommendations on how one can best simulate light for the Geometric optics model.

Chapter 1

Geometric Optics

In this chapter, we will introduce mathematical concepts of Geometric optics. The eikonal equation will be introduced and explained. In order to do that, we start with defining some properties of rays.

1.1 Eikonal equation

We consider a light ray as a piecewise smooth curve $\mathcal{C}$ from a point P_0 to P_1, with coordinates $\boldsymbol{x}_0$ and $\boldsymbol{x}_1$. Obviously, $\boldsymbol{x}_0$ and $\boldsymbol{x}_1$ are elements from $\mathbb{R}^3$. For the curve $\mathcal{C}$, consider the parametrization $\boldsymbol{x}(\tau),\ \tau_0 \leq \tau \leq \tau_1$ with $\boldsymbol{x}(\tau_0) = \boldsymbol{x}_0$ and $\boldsymbol{x}(\tau_1) = \boldsymbol{x}_1$ [3]. The light ray then has a *geometric length*, or *arc-length*, s, given by [4]

$$s(\boldsymbol{x}_0, \boldsymbol{x}_1) = \int_{\mathcal{C}} \mathrm{d}s = \int_{\tau_0}^{\tau_1} |\boldsymbol{x}'(\tau)| \, \mathrm{d}\tau. \tag{1.1}$$

The path also has an *optical path length*. The optical path length is the product of the geometric path length and the index of refraction n. The refractive index is defined as

$$n = \frac{c}{v}, \tag{1.2}$$

where c is the constant speed of light in vacuum and v is the speed of light in the current medium. Because the medium can be different at positions $\boldsymbol{x}$, we consider the refractive index as a function of $\boldsymbol{x}$, i.e., $n = n(\boldsymbol{x})$. Therefore, the optical path length $\psi(\boldsymbol{x}_0, \boldsymbol{x}_1)$ is given by the following line integral

$$\psi(\boldsymbol{x}_0, \boldsymbol{x}_1) = \int_{\mathcal{C}} n(\boldsymbol{x}) \ \mathrm{d}s. \tag{1.3}$$

Using the parametrization for the curve $\mathcal{C}$, we obtain

$$\psi(\boldsymbol{x}_0, \boldsymbol{x}_1) = \int_{\tau_0}^{\tau_1} n(\boldsymbol{x}(\tau)) \, |\boldsymbol{x}'(\tau)| \ \mathrm{d}\tau. \tag{1.4}$$

A fundamental principle in Geometric optics for a light ray is *Fermat's principle*. The principle implies that the optical path length of rays between P_0 and P_1 is stationary with respect to infinitesimal variations of the curve $\mathcal{C}$ [3]. In particular, Fermat's principle

implies that equation (1.3) attains a minimum or a saddle point, because maxima never occur.

We introduce the function $\psi(\boldsymbol{x}) = \psi(\boldsymbol{x}_0, \boldsymbol{x})$ for the optical length between the fixed point $\boldsymbol{x}_0$ and the variable point $\boldsymbol{x}$.

Besides rays, we will also introduce so-called *geometric wavefronts*. A geometric wavefront is defined as a surface for which the optical path length is constant. In other words, a surface for which

$$\psi(\boldsymbol{x}) = c_1, \tag{1.5}$$

for some constant c_1. Later, we will see that these wavefronts are perpendicular to the rays. Figure 1.1 illustrates what wavefronts look like.

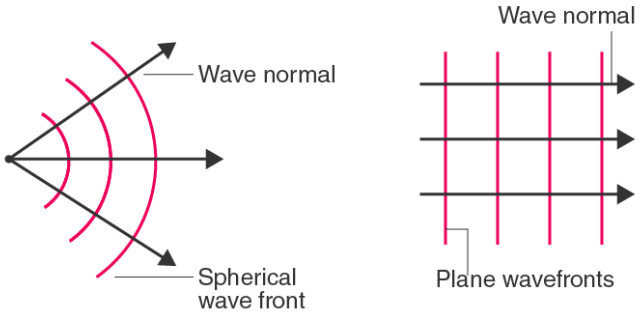

Figure 1.1: Wavefronts and rays for a point-source (left) and a plane wave (right).

The wavefront can also be characterised by means of the time t. The wavefront after time t is given by

$$\psi(\boldsymbol{x}(t)) = c(t - t_0), \tag{1.6}$$

for constant c as the speed of light in vacuum. We take $t_0 = 0$, such that rays start at $\boldsymbol{x}_0 = \boldsymbol{x}(0)$ at $t = 0$. Using expression (1.6), we can characterise the light source as the surface $\psi(\boldsymbol{x}) = 0$.

Throughout this chapter, we will be concerned with the *eikonal equation*. The eikonal equation is a non-linear partial differential equation (PDE), that can be obtained from the wave equation under the assumptions of the Geometric optics model [3]. In particular, it is a first-order nonlinear PDE and reads

$$|\nabla\psi(\boldsymbol{x})| = n(\boldsymbol{x}), \qquad \boldsymbol{x} \in \Omega, \tag{1.7a}$$
$$\psi(\boldsymbol{x}) = f(\boldsymbol{x}), \qquad \boldsymbol{x} \in \partial\Omega, \tag{1.7b}$$

with domain Ω and boundary conditions $f(\boldsymbol{x})$ for the boundary $\partial\Omega$. The eikonal equation will be transformed into a system of ordinary differential equations (ODEs). To transform the equation into a system of ODEs, the so-called method of characteristics is used.

1.2 The method of characteristics

In this section, a general formulation of the *method of characteristics* is given. After that, the method is applied to the earlier proposed eikonal equation (1.7). At the end of this section we will have characterised the rays and wavefronts.

The method of characteristics considers a nonlinear first-order partial differential equation for the unknown $u = u(\boldsymbol{x})$ of form

$$F(\boldsymbol{x}, u, \boldsymbol{p}) = 0, \qquad \boldsymbol{p} = \nabla u. \tag{1.8}$$

Hence, $\boldsymbol{x}$ is the position vector and $\boldsymbol{p}$ is the gradient vector of u. The solution of PDE (1.8) can be found by solving the related system of ODEs, known as the *characteristic system*, given by

$$\frac{\mathrm{d}\boldsymbol{x}}{\mathrm{d}s} = \frac{\partial F}{\partial \boldsymbol{p}}, \tag{1.9a}$$

$$\frac{\mathrm{d}u}{\mathrm{d}s} = \boldsymbol{p} \cdot \frac{\partial F}{\partial \boldsymbol{p}}, \tag{1.9b}$$

$$\frac{\mathrm{d}\boldsymbol{p}}{\mathrm{d}s} = -\boldsymbol{p}\frac{\partial F}{\partial u} - \frac{\partial F}{\partial \boldsymbol{x}}. \tag{1.9c}$$

A *characteristic* is defined as the curve parametrized by $\boldsymbol{x} = \boldsymbol{x}(s),\ s \in I$ for some interval I and some parameter s. The unknown u and its gradient $\boldsymbol{p}$ can be solved *along* the characteristic. The solution of ODE system (1.9) can only be found by integrating the ODEs simultaneously over the parameter s. A derivation of (1.9) is given.

Because u and $\boldsymbol{p}$ are solved along the characteristic, we can express u and $\boldsymbol{p}$ in terms of s as follows

$$u(s) = u(\boldsymbol{x}(s)), \tag{1.10a}$$

$$\boldsymbol{p}(s) = \boldsymbol{p}(\boldsymbol{x}(s)). \tag{1.10b}$$

Differentiating these using the chain rule gives

$$\frac{\mathrm{d}u}{\mathrm{d}s} = \sum_{j=1}^{d} \frac{\partial u}{\partial x_j}\frac{\mathrm{d}x_j}{\mathrm{d}s} = \nabla u \cdot \frac{\mathrm{d}\boldsymbol{x}}{\mathrm{d}s} = \boldsymbol{p} \cdot \frac{\mathrm{d}\boldsymbol{x}}{\mathrm{d}s}, \tag{1.11a}$$

$$\frac{\mathrm{d}p_i}{\mathrm{d}s} = \sum_{j=1}^{d} \frac{\partial p_i}{\partial x_j}\frac{\mathrm{d}x_j}{\mathrm{d}s} = \sum_{j=1}^{d} \frac{\partial p_j}{\partial x_i}\frac{\mathrm{d}x_j}{\mathrm{d}s} = \frac{\partial \boldsymbol{p}}{\partial x_i} \cdot \frac{\mathrm{d}\boldsymbol{x}}{\mathrm{d}s}. \tag{1.11b}$$

The variable d denotes the dimension of $\boldsymbol{x}$. In equation (1.11b), we assume that $u(\boldsymbol{x})$ has continuous second-order partial derivatives in the domain, such that we can change the order of differentiation. In order to make a proper choice for $\mathrm{d}\boldsymbol{x}/\mathrm{d}s$ (and hence the parameters), the derivative of $F(\boldsymbol{x}, u, \boldsymbol{p}) = 0$ with respect to x_i is taken and is given

by

$$\frac{\partial F}{\partial x_i} + \frac{\partial F}{\partial u}\, p_i + \frac{\partial F}{\partial \boldsymbol{p}} \cdot \frac{\partial \boldsymbol{p}}{\partial x_i} = 0. \tag{1.12}$$

Comparing (1.11b) and (1.12) gives rise to the choice

$$\frac{\mathrm{d}\boldsymbol{x}}{\mathrm{d}s} = \frac{\partial F}{\partial \boldsymbol{p}}. \tag{1.13}$$

This choice implies that equations (1.11a) and (1.11b), using (1.12), become

$$\frac{\mathrm{d}u}{\mathrm{d}s} = \boldsymbol{p} \cdot \frac{\partial F}{\partial \boldsymbol{p}}, \tag{1.14a}$$

$$\frac{\mathrm{d}p_i}{\mathrm{d}s} = \frac{\partial \boldsymbol{p}}{\partial x_i} \cdot \frac{\partial F}{\partial \boldsymbol{p}} = -p_i \frac{\partial F}{\partial u} - \frac{\partial F}{\partial x_i}. \tag{1.14b}$$

Hence, the system of ODEs (1.9) is found, and the formulated method of characteristics can be applied to the eikonal equation.

The eikonal equation (1.7) in the form (1.8) reads

$$F(\boldsymbol{x}, \psi, \boldsymbol{p}) = |\boldsymbol{p}| - n(\boldsymbol{x}) = 0, \qquad \boldsymbol{p} = \nabla\psi. \tag{1.15}$$

Hence, the method of characteristics states that the characteristic system reads

$$\frac{\mathrm{d}\boldsymbol{x}}{\mathrm{d}s} = \frac{\boldsymbol{p}}{n}, \tag{1.16a}$$

$$\frac{\mathrm{d}\psi}{\mathrm{d}s} = n, \tag{1.16b}$$

$$\frac{\mathrm{d}\boldsymbol{p}}{\mathrm{d}s} = \nabla n. \tag{1.16c}$$

Together with initial conditions, ODE system (1.16) represents the solution of one characteristic. Although it might seem like this characteristic is very abstract, it is in fact not, because the characteristics coincide with the rays. In order words, the solution of ODE system (1.16) mathematically defines a ray.

Furthermore, it can be observed that equation (1.16a) implies the following

$$\left|\frac{\mathrm{d}\boldsymbol{x}}{\mathrm{d}s}\right| = \frac{|\boldsymbol{p}|}{n} = 1, \tag{1.17}$$

which tells us that the variable s is the arc-length along the characteristic. This is the same as the geometric path length as described in (1.1). In order words, this means that $\mathrm{d}s$ can be considered as an infinitesimal length element along the path of the ray.

A particular equation, called the *ray equation*, will be used later in the report. Combining equation (1.16a) and the fact that we used $\boldsymbol{p} = \nabla\psi$, we have

$$n\,\frac{\mathrm{d}\boldsymbol{x}}{\mathrm{d}s} = \nabla\psi. \tag{1.18}$$

Differentiation of (1.18) with respect to s, using (1.16c), gives the ray equation and reads

$$\frac{\mathrm{d}}{\mathrm{d}s}\left(n\,\frac{\mathrm{d}\boldsymbol{x}}{\mathrm{d}s}\right) = \nabla n. \tag{1.19}$$

In Chapter 4, we will describe cross-sections of lenses, which is done by considering the plane $z = C$ for some constant C. In that case, the eikonal equation (1.7) together with the characteristic system (1.16) are two-dimensional. In particular, this means that $\boldsymbol{x} = (x, y)^T$ and $\boldsymbol{p} = (p_1, p_2)^T$ for $p_1 = \partial\psi/\partial x$ and $p_2 = \partial\psi/\partial y$. Using this, we can write eikonal equation (1.7) in two-dimensional form as

$$\sqrt{p_1^2 + p_2^2} = n(x, y), \tag{1.20}$$

and the corresponding characteristic system reads

$$\frac{\mathrm{d}x}{\mathrm{d}s} = \frac{p_1}{n}, \qquad \frac{\mathrm{d}y}{\mathrm{d}s} = \frac{p_2}{n}, \tag{1.21a}$$

$$\frac{\mathrm{d}\psi}{\mathrm{d}s} = n, \tag{1.21b}$$

$$\frac{\mathrm{d}p_1}{\mathrm{d}s} = \frac{\partial n}{\partial x}, \qquad \frac{\mathrm{d}p_2}{\mathrm{d}s} = \frac{\partial n}{\partial y}. \tag{1.21c}$$

Observe that (1.21b) corresponds with the earlier defined optical path length (1.3).

Some papers consider a squared form of the eikonal equation, i.e., [5]

$$F(\boldsymbol{x}, \psi, \boldsymbol{p}) = |\boldsymbol{p}|^2 - n^2(\boldsymbol{x}), \tag{1.22}$$

which gives the more pleasant expanded form

$$p_1^2 + p_2^2 = n^2(x, y). \tag{1.23}$$

We apply the method of characteristics to equation (1.22). Along the characteristic $\boldsymbol{x} = \boldsymbol{x}(\tau)$ for some parameter τ, we then get the system of ODEs given by

$$\frac{\mathrm{d}x}{\mathrm{d}\sigma} = 2p_1, \qquad \frac{\mathrm{d}y}{\mathrm{d}\sigma} = 2p_2, \tag{1.24a}$$

$$\frac{\mathrm{d}\psi}{\mathrm{d}\sigma} = 2n^2, \tag{1.24b}$$

$$\frac{\mathrm{d}p_1}{\mathrm{d}\sigma} = 2n\,\frac{\partial n}{\partial x}, \qquad \frac{\mathrm{d}p_2}{\mathrm{d}\sigma} = 2n\,\frac{\partial n}{\partial y}. \tag{1.24c}$$

This is in fact system (1.21) in disguise. If we divide by $2n$ on both sides for each equation in (1.24), we obtain the following

$$\frac{1}{2n}\frac{\mathrm{d}x}{\mathrm{d}\sigma} = \frac{p_1}{n}, \qquad \frac{1}{2n}\frac{\mathrm{d}y}{\mathrm{d}\sigma} = \frac{p_2}{n}, \tag{1.25a}$$

$$\frac{1}{2n}\frac{\mathrm{d}\psi}{\mathrm{d}\sigma} = n, \tag{1.25b}$$

$$\frac{1}{2n}\frac{\mathrm{d}p_1}{\mathrm{d}\sigma} = \frac{\partial n}{\partial x}, \qquad \frac{1}{2n}\frac{\mathrm{d}p_2}{\mathrm{d}\sigma} = \frac{\partial n}{\partial y}. \tag{1.25c}$$

Together with system (1.21) we conclude the following

$$2n\,\mathrm{d}\sigma = \mathrm{d}s, \tag{1.26}$$

which means that the parameter σ can be described as

$$\sigma = \int_{\mathcal{C}} \frac{1}{2n(\boldsymbol{x})}\,\mathrm{d}s. \tag{1.27}$$

Equation (1.26) describes the relation between the parameters σ and s. We can conclude that the eikonal equation and its squared variant, as expected, give the same characteristic system.

Up till now we have mainly focused on the characteristic system using the parameter s. This parameter s has a physical meaning, because it is the geometric path length of the light ray. We have seen that ψ is a function of s along the characteristic and in particular, from equation (1.21b), we can deduce the following

$$\mathrm{d}\psi = n\,\mathrm{d}s, \tag{1.28}$$

or equivalently

$$\frac{\mathrm{d}s}{\mathrm{d}\psi} = \frac{1}{n}. \tag{1.29}$$

By multiplying each side of (1.29) with each side of system (1.21), we obtain a new system which reads

$$\frac{\mathrm{d}x}{\mathrm{d}\psi} = \frac{p_1}{n^2}, \qquad \frac{\mathrm{d}y}{\mathrm{d}\psi} = \frac{p_2}{n^2}, \tag{1.30a}$$

$$\frac{\mathrm{d}p_1}{\mathrm{d}\psi} = \frac{1}{n}\frac{\partial n}{\partial x}, \qquad \frac{\mathrm{d}p_2}{\mathrm{d}\psi} = \frac{1}{n}\frac{\partial n}{\partial y}. \tag{1.30b}$$

This means we have found a second characteristic system having a physical meaning, because the parameter ψ is the optical path length of the light ray. When we use a numerical time integration method to approximate the solution of system (1.30), any ray at step i will have the same optical path length. This holds for a fixed step size h. Therefore, by simulating enough rays, a wavefront can be simulated as the surface $\psi(\boldsymbol{x}) = ih$, for any i. Hence, characteristic system (1.30) can be used to approximate the wavefronts.

Using equation (1.6), we can now give a characteristic system in terms of the parameter t, the physical time. This system is simply given by

$$\frac{\mathrm{d}x}{\mathrm{d}t} = \frac{c\,p_1}{n^2}, \qquad \frac{\mathrm{d}y}{\mathrm{d}t} = \frac{c\,p_2}{n^2}, \tag{1.31a}$$

$$\frac{\mathrm{d}\psi}{\mathrm{d}t} = c, \tag{1.31b}$$

$$\frac{\mathrm{d}p_1}{\mathrm{d}t} = \frac{c}{n}\frac{\partial n}{\partial x}, \qquad \frac{\mathrm{d}p_2}{\mathrm{d}t} = \frac{c}{n}\frac{\partial n}{\partial y}. \tag{1.31c}$$

1.3 Polar coordinates

Polar coordinates can be expressed by the distance to the origin r and the angle ϕ, which is the angle between the position vector and the positive x-axis. The relation between Cartesian and polar coordinates can be described as

$$x = r\cos(\phi), \quad y = r\sin(\phi), \quad r \geq 0, \quad 0 \leq \phi < 2\pi. \tag{1.32}$$

For spherical and cylindrical symmetric lenses, the refractive index function can be written as $n = n(r)$. For such lenses, it is very natural to describe the rays in terms of polar coordinates. In this section we will transform the eikonal equation and its characteristic system into polar coordinates. In Chapter 4, examples of such spherical and cylindrical symmetric lenses will be given.

The gradient of ψ can be described in polar coordinates as [6]

$$\nabla\psi = \frac{\partial\psi}{\partial r}\,\hat{\mathbf{e}}_r + \frac{1}{r}\frac{\partial\psi}{\partial\phi}\,\hat{\mathbf{e}}_\phi, \tag{1.33}$$

with orthogonal unit vectors $\hat{\mathbf{e}}_r$ and $\hat{\mathbf{e}}_\phi$. These vectors are given by

$$\hat{\mathbf{e}}_r = \begin{pmatrix}\cos\phi\\ \sin\phi\end{pmatrix}, \qquad \hat{\mathbf{e}}_\phi = \begin{pmatrix}-\sin\phi\\ \cos\phi\end{pmatrix}. \tag{1.34}$$

In addition, the relation between the partial derivatives of ψ in polar coordinates and Cartesian coordinates, is as follows

$$\frac{\partial\psi}{\partial r} = \frac{\partial\psi}{\partial x}\frac{\partial x}{\partial r} + \frac{\partial\psi}{\partial y}\frac{\partial y}{\partial r} = \frac{\partial\psi}{\partial x}\cos(\phi) + \frac{\partial\psi}{\partial y}\sin(\phi), \tag{1.35a}$$

$$\frac{\partial\psi}{\partial\phi} = \frac{\partial\psi}{\partial x}\frac{\partial x}{\partial\phi} + \frac{\partial\psi}{\partial y}\frac{\partial y}{\partial\phi} = -\frac{\partial\psi}{\partial x}\,r\sin(\phi) + \frac{\partial\psi}{\partial y}\,r\cos(\phi). \tag{1.35b}$$

Because $\boldsymbol{p} = \nabla\psi$ by definition, we have the following polar expression for $\boldsymbol{p}$

$$\boldsymbol{p} = p_r\,\hat{\mathbf{e}}_r + p_\phi\,\hat{\mathbf{e}}_\phi, \tag{1.36}$$

for

$$p_r = \frac{\partial \psi}{\partial r}, \qquad p_\phi = \frac{1}{r}\frac{\partial \psi}{\partial \phi}. \tag{1.37}$$

The characteristic can be expressed as

$$\boldsymbol{x}(s) = r\,(s)\;\hat{\mathbf{e}}_r\,(\phi(s))\,,\;\; s \in I, \tag{1.38}$$

for some interval I. The characteristic equations should describe the dynamics of the parameters r, ϕ, ψ, p_r and p_ϕ. Starting with the first two, the position vector $\boldsymbol{x}$ in polar form is written as

$$\boldsymbol{x} = r\,\hat{\mathbf{e}}_r. \tag{1.39}$$

Differentiating the position vector with respect to s gives

$$\frac{\mathrm{d}\boldsymbol{x}}{\mathrm{d}s} = \frac{\mathrm{d}r}{\mathrm{d}s}\,\hat{\mathbf{e}}_r + r\,\frac{\mathrm{d}\hat{\mathbf{e}}_r}{\mathrm{d}s}, \tag{1.40}$$

where

$$\frac{\mathrm{d}\hat{\mathbf{e}}_r}{\mathrm{d}s} = \begin{pmatrix} -\sin\phi \\ \cos\phi \end{pmatrix}\frac{\mathrm{d}\phi}{\mathrm{d}s} = \frac{\mathrm{d}\phi}{\mathrm{d}s}\,\hat{\mathbf{e}}_\phi. \tag{1.41}$$

Combining equations (1.40) and (1.41) gives

$$\frac{\mathrm{d}\boldsymbol{x}}{\mathrm{d}s} = \frac{\mathrm{d}r}{\mathrm{d}s}\hat{\mathbf{e}}_r + r\frac{\mathrm{d}\phi}{\mathrm{d}s}\hat{\mathbf{e}}_\phi. \tag{1.42}$$

On the other hand, the position vector $\boldsymbol{x}$ was earlier expressed in (1.16) as

$$\frac{\mathrm{d}\boldsymbol{x}}{\mathrm{d}s} = \frac{\boldsymbol{p}}{n} = \frac{1}{n}\left(p_r\,\hat{\mathbf{e}}_r + p_\phi\,\hat{\mathbf{e}}_\phi\right). \tag{1.43}$$

Comparing the right hand sides of (1.42) and (1.43), gives rise to the following ODEs.

$$\frac{\mathrm{d}r}{\mathrm{d}s} = \frac{p_r}{n}, \qquad \frac{\mathrm{d}\phi}{\mathrm{d}s} = \frac{p_\phi}{nr}. \tag{1.44}$$

What remains is to get an expression for $\mathrm{d}p_r/\mathrm{d}s$ and $\mathrm{d}p_\phi/\mathrm{d}s$. The procedure is very similar as before, but now we look at the $\boldsymbol{p}$-vector. First, we differentiate equation (1.36) with respect to s, giving

$$\frac{\mathrm{d}\boldsymbol{p}}{\mathrm{d}s} = \frac{\mathrm{d}p_r}{\mathrm{d}s}\,\hat{\mathbf{e}}_r + p_r\,\frac{\mathrm{d}\hat{\mathbf{e}}_r}{\mathrm{d}s} + \frac{\mathrm{d}p_\phi}{\mathrm{d}s}\,\hat{\mathbf{e}}_\phi + p_\phi\,\frac{\mathrm{d}\hat{\mathbf{e}}_\phi}{\mathrm{d}s}, \tag{1.45}$$

where

$$\frac{\mathrm{d}\hat{\mathbf{e}}_\phi}{\mathrm{d}s} = \begin{pmatrix} -\cos\phi \\ -\sin\phi \end{pmatrix}\frac{\mathrm{d}\phi}{\mathrm{d}s} = -\hat{\mathbf{e}}_r\frac{\mathrm{d}\phi}{\mathrm{d}s}. \tag{1.46}$$

Next, we substitute equation (1.46) and (1.41) into equation (1.45). The remaining equation can be written as

$$\frac{\mathrm{d}\boldsymbol{p}}{\mathrm{d}s} = \left(\frac{\mathrm{d}p_r}{\mathrm{d}s} - p_\phi \frac{\mathrm{d}\phi}{\mathrm{d}s}\right)\hat{\mathbf{e}}_r + \left(\frac{\mathrm{d}p_\phi}{\mathrm{d}s} + p_r \frac{\mathrm{d}\phi}{\mathrm{d}s}\right)\hat{\mathbf{e}}_\phi. \tag{1.47}$$

Now, consider the characteristic equation (1.16c) from the Cartesian coordinate system. In polar coordinates, the gradient of n only has a component in the $\hat{\mathbf{e}}_r$-direction, because $n = n(r)$ by assumption. So the following holds

$$\frac{\mathrm{d}\boldsymbol{p}}{\mathrm{d}s} = \nabla n = \frac{\mathrm{d}n}{\mathrm{d}r}\hat{\mathbf{e}}_r. \tag{1.48}$$

Observe that the right-hand side of equations (1.47) and (1.48) should be equal. This gives rise to the following ODEs.

$$\frac{\mathrm{d}p_r}{\mathrm{d}s} = p_\phi \frac{\mathrm{d}\phi}{\mathrm{d}s} + \frac{\mathrm{d}n}{\mathrm{d}r}, \tag{1.49a}$$

$$\frac{\mathrm{d}p_\phi}{\mathrm{d}s} = -p_r \frac{\mathrm{d}\phi}{\mathrm{d}s}. \tag{1.49b}$$

Using the ODEs from (1.44), this reduces to

$$\frac{\mathrm{d}p_r}{\mathrm{d}s} = \frac{p_\phi^2}{nr} + \frac{\mathrm{d}n}{\mathrm{d}r}, \qquad \frac{\mathrm{d}p_\phi}{\mathrm{d}s} = -\frac{p_r\, p_\phi}{nr}. \tag{1.50}$$

Finally, the dynamics of the parameter ψ is the same as in Cartesian coordinates and is given by

$$\frac{\mathrm{d}\psi}{\mathrm{d}s} = n(r). \tag{1.51}$$

Summarizing, the system of ODEs characterising the eikonal equation (1.7) in polar coordinates can be written as

$$\frac{\mathrm{d}r}{\mathrm{d}s} = \frac{p_r}{n}, \qquad \frac{\mathrm{d}\phi}{\mathrm{d}s} = \frac{p_\phi}{nr}, \tag{1.52a}$$

$$\frac{\mathrm{d}\psi}{\mathrm{d}s} = n, \tag{1.52b}$$

$$\frac{\mathrm{d}p_r}{\mathrm{d}s} = \frac{p_\phi^2}{nr} + \frac{\mathrm{d}n}{\mathrm{d}r}, \qquad \frac{\mathrm{d}p_\phi}{\mathrm{d}s} = -\frac{p_r\, p_\phi}{nr}. \tag{1.52c}$$

For the squared eikonal equation in polar coordinates, one can obtain a similar system of ODEs for parameter σ instead of s.

To conclude this section, an overview of the main results from this chapter are given on the next page.

1.4 Overview

Cartesian Coordinate System	**Polar Coordinate System**
Eikonal equation $\lvert\nabla\psi(x,y)\rvert = n(x,y)$	 $\lvert\nabla\psi(r,\phi)\rvert = n(r)$
Characteristic system For s, the arc-length of the light ray. $\frac{\mathrm{d}x}{\mathrm{d}s} = \frac{p_1}{n}, \quad \frac{\mathrm{d}y}{\mathrm{d}s} = \frac{p_2}{n},$ $\frac{\mathrm{d}\psi}{\mathrm{d}s} = n,$ $\frac{\mathrm{d}p_1}{\mathrm{d}s} = \frac{\partial n}{\partial x}, \quad \frac{\mathrm{d}p_2}{\mathrm{d}s} = \frac{\partial n}{\partial y}.$	 $\frac{\mathrm{d}r}{\mathrm{d}s} = \frac{p_r}{n}, \quad \frac{\mathrm{d}\phi}{\mathrm{d}s} = \frac{p_\phi}{nr},$ $\frac{\mathrm{d}\psi}{\mathrm{d}s} = n,$ $\frac{\mathrm{d}p_r}{\mathrm{d}s} = \frac{p_\phi^2}{nr} + \frac{\partial n}{\partial r}, \quad \frac{\mathrm{d}p_\phi}{\mathrm{d}s} = -\frac{p_r\, p_\phi}{nr}.$
Characteristic system For ψ, the optical path length of the light ray. $\frac{\mathrm{d}x}{\mathrm{d}\psi} = \frac{p_1}{n^2}, \quad \frac{\mathrm{d}y}{\mathrm{d}\psi} = \frac{p_2}{n^2},$ $\frac{\mathrm{d}p_1}{\mathrm{d}\psi} = \frac{1}{n}\frac{\partial n}{\partial x}, \quad \frac{\mathrm{d}p_2}{\mathrm{d}\psi} = \frac{1}{n}\frac{\partial n}{\partial y}.$	 $\frac{\mathrm{d}r}{\mathrm{d}\psi} = \frac{p_r}{n^2}, \quad \frac{\mathrm{d}\phi}{\mathrm{d}\psi} = \frac{p_\phi}{n^2\, r},$ $\frac{\mathrm{d}p_r}{\mathrm{d}\psi} = \frac{p_\phi^2}{n^2\, r} + \frac{1}{n}\frac{\partial n}{\partial r}, \quad \frac{\mathrm{d}p_\phi}{\mathrm{d}\psi} = -\frac{p_r\, p_\phi}{n^2\, r}.$
Characteristic system For t, the physical time. $\frac{\mathrm{d}x}{\mathrm{d}t} = \frac{c\, p_1}{n^2}, \quad \frac{\mathrm{d}y}{\mathrm{d}t} = \frac{c\, p_2}{n^2},$ $\frac{\mathrm{d}\psi}{\mathrm{d}t} = c,$ $\frac{\mathrm{d}p_1}{\mathrm{d}t} = \frac{c}{n}\frac{\partial n}{\partial x}, \quad \frac{\mathrm{d}p_2}{\mathrm{d}t} = \frac{c}{n}\frac{\partial n}{\partial y}.$	 $\frac{\mathrm{d}r}{\mathrm{d}t} = \frac{c\, p_r}{n^2}, \quad \frac{\mathrm{d}\phi}{\mathrm{d}t} = \frac{c\, p_\phi}{n^2\, r},$ $\frac{\mathrm{d}\psi}{\mathrm{d}t} = c,$ $\frac{\mathrm{d}p_r}{\mathrm{d}t} = \frac{c\, p_\phi^2}{n^2\, r} + \frac{c}{n}\frac{\partial n}{\partial r}, \quad \frac{\mathrm{d}p_\phi}{\mathrm{d}t} = -\frac{c\, p_r\, p_\phi}{n^2\, r}.$

Chapter 2

Hamiltonian Optics

In this chapter we consider a more specific formulation of Geometric Optics, called *Hamiltonian Optics*. Hamiltonian Optics uses mathematical concepts from Hamiltonian Mechanics, first formulated by William Rowan Hamilton in 1833. It is a reformulation of Lagrangian Mechanics, introduced by Joseph Louis Lagrange in 1788.

In this chapter, the characteristic system describing the light rays will be written as a Hamiltonian system. The flow of such a system is *symplectic*. This means that it is area preserving the phase space, which is the set of all possible solutions of the ODE system. There exist special numerical methods that inherit this property, making them in general more suitable.

A Hamiltonian system is generated by a Hamiltonian $\mathcal{H} = \mathcal{H}(\boldsymbol{q}, \boldsymbol{p})$. The Hamiltonian depends on the position vector $\boldsymbol{q}$ and the momentum vector $\boldsymbol{p}$. The corresponding Hamiltonian system reads

$$\frac{\mathrm{d}\boldsymbol{q}}{\mathrm{d}\tau} = \frac{\partial \mathcal{H}}{\partial \boldsymbol{p}}, \tag{2.1a}$$

$$\frac{\mathrm{d}\boldsymbol{p}}{\mathrm{d}\tau} = -\frac{\partial \mathcal{H}}{\partial \boldsymbol{q}}, \tag{2.1b}$$

for some parameter τ. This means that we have to convert the earlier found characteristic system to this form, to find the underlying Hamiltonian.

2.1 Cartesian coordinates

In Cartesian coordinates, we have to find a Hamiltonian for the ODE system (1.21). Therefore, let $\boldsymbol{q} = (x, y)^T$ and $\boldsymbol{p} = (p_1, p_2)^T$. Observe that equations (1.21a) and (1.21c) can be written as

$$\frac{\mathrm{d}\boldsymbol{q}}{\mathrm{d}s/n} = \boldsymbol{p}, \tag{2.2a}$$

$$\frac{\mathrm{d}\boldsymbol{p}}{\mathrm{d}s/n} = n(\boldsymbol{q})\,\nabla n(\boldsymbol{q}). \tag{2.2b}$$

Introducing the Hamiltonian

$$\mathcal{H}(\boldsymbol{q}, \boldsymbol{p}) = \frac{|\boldsymbol{p}|^2}{2} - \frac{n^2(\boldsymbol{q})}{2}, \tag{2.3}$$

we find a Hamiltonian system, given by

$$\frac{\mathrm{d}\boldsymbol{q}}{\mathrm{d}\tau} = \boldsymbol{p}, \tag{2.4a}$$

$$\frac{\mathrm{d}\boldsymbol{p}}{\mathrm{d}\tau} = n(\boldsymbol{q})\,\nabla n(\boldsymbol{q}), \tag{2.4b}$$

with $\mathrm{d}\tau = \mathrm{d}s/n$. Using the result from (1.26), we have

$$\frac{\mathrm{d}s}{\mathrm{d}\tau} = n, \tag{2.5a}$$

$$\frac{\mathrm{d}s}{\mathrm{d}\sigma} = 2n. \tag{2.5b}$$

From this, we can conclude that we have the relation between parameters $\tau = 2\sigma$, where σ is the parameter from the characteristic system (1.24).

Using equation (2.5a), the optical path length for parameter τ can be given by

$$\frac{\mathrm{d}\psi}{\mathrm{d}\tau} = n^2. \tag{2.6}$$

For the two-dimensional eikonal equation, we can expand the Hamiltonian $\mathcal{H} = \mathcal{H}(x, y, p_1, p_2)$ as

$$\mathcal{H} = \frac{p_1^2 + p_2^2}{2} - \frac{n^2}{2}, \tag{2.7}$$

with Hamiltonian system

$$\frac{\mathrm{d}x}{\mathrm{d}\tau} = p_1, \qquad \frac{\mathrm{d}y}{\mathrm{d}\tau} = p_2, \tag{2.8a}$$

$$\frac{\mathrm{d}p_1}{\mathrm{d}\tau} = n\,\frac{\partial n}{\partial x}, \qquad \frac{\mathrm{d}p_2}{\mathrm{d}\tau} = n\,\frac{\partial n}{\partial y}. \tag{2.8b}$$

Finally, we can observe that Hamiltonian (2.3) can be written as

$$\mathcal{H}(\boldsymbol{p}, \boldsymbol{q}) = T(\boldsymbol{p}) + V(\boldsymbol{q}). \tag{2.9}$$

These kind of Hamiltonians are part of a special class called *separable* Hamiltonians. A separable Hamiltonian has advantages in certain time integration methods, which will become clear in Chapter 3.

2.2 Polar coordinates

Next, we investigate what the Hamiltonian system looks like in polar coordinates. We recall that the position vector $\boldsymbol{q}$ and momentum vector $\boldsymbol{p}$ in polar coordinates are given as

$$\boldsymbol{q} = r\,\hat{\mathbf{e}}_r(\phi), \tag{2.10a}$$
$$\boldsymbol{p} = p_r\,\hat{\mathbf{e}}_r + p_\phi\,\hat{\mathbf{e}}_\phi. \tag{2.10b}$$

Hence, we have that

$$|\boldsymbol{p}|^2 = p_r^2 + p_\phi^2. \tag{2.11}$$

To determine the Hamiltonian system we have to express system (2.4) in polar coordinates. Using equation (1.42) and (2.10b), we obtain the ODEs for r and ϕ, given by

$$\frac{\mathrm{d}r}{\mathrm{d}\tau} = p_r, \qquad r\,\frac{\mathrm{d}\phi}{\mathrm{d}\tau} = p_\phi. \tag{2.12}$$

Analogously, by using equations (1.47) and the expression for ∇n from equation (1.48), we obtain the ODEs for p_r and p_ϕ, given by

$$\frac{\mathrm{d}p_r}{\mathrm{d}\tau} = \frac{p_\phi^2}{r} + n\frac{\mathrm{d}n}{\mathrm{d}r}, \qquad r\,\frac{\mathrm{d}p_\phi}{\mathrm{d}\tau} = -p_r\,p_\phi. \tag{2.13}$$

This means that the Hamiltonian system reads

$$\frac{\mathrm{d}r}{\mathrm{d}\tau} = p_r, \qquad r\,\frac{\mathrm{d}\phi}{\mathrm{d}\tau} = p_\phi, \tag{2.14a}$$
$$\frac{\mathrm{d}p_r}{\mathrm{d}\tau} = \frac{p_\phi^2}{r} + n\frac{\mathrm{d}n}{\mathrm{d}r}, \qquad r\,\frac{\mathrm{d}p_\phi}{\mathrm{d}\tau} = -p_r\,p_\phi. \tag{2.14b}$$

Using the parameter relation (2.5a), we can verify that the Hamiltonian system (2.14) together with (2.6) is a reparametrization of the earlier found characteristic system (1.52).

At this point, we have fully determined what the Hamiltonian looks like. It makes sense to elaborate a bit more on the usefulness of this topic. In the next chapter, several time integration methods will be presented. Some of these methods use the Hamiltonian

system to approximate the rays. In Chapter 5, the numerical methods will be compared to each other. The Hamiltonian introduces a method of comparing these different numerical methods. From the eikonal equation (1.7) itself, we can conclude that the constant value of the Hamiltonian $\mathcal{H}$ is equal to zero. Therefore, we can calculate the Hamiltonian for a numerical method at each integration step. More on this will follow in Chapter 5.

Chapter 3

Time integration methods

We have seen quite some systems of ODEs, that all characterise the eikonal equation. We like to approximate the solution of the systems of ODEs using time integration schemes. In this chapter, several time integration schemes will be presented. The first two are basic Euler schemes, followed by two symplectic schemes. After that, a Runge-Kutta scheme and Gauss-Legendre scheme will be given. We start with introducing some notation for the numerical methods in general.

Consider a general system of ODEs

$$\boldsymbol{y}' = \boldsymbol{f}(t, \boldsymbol{y}), \quad t > 0, \tag{3.1a}$$

$$\boldsymbol{y}(0) = \boldsymbol{y}_0, \tag{3.1b}$$

where prime ($'$) denotes differentiation with respect to t. In system (3.1), $\boldsymbol{y}$ is a vector of unknowns, $\boldsymbol{f}$ is a vector field and $\boldsymbol{y}_0$ is a vector containing initial conditions for the unknowns in $\boldsymbol{y}$.

We introduce the discrete time levels

$$t_i = ih, \quad i = 0, 1, \ldots \tag{3.2}$$

with $h > 0$ as step size. A numerical method approximates the ODEs (3.1a) at $t = t_i$. The numerical approximation of $\boldsymbol{y}$ at t_i is denoted by $\boldsymbol{y}_i$.

For the system of ODEs (2.8), the solution $\boldsymbol{y}$ is given by

$$\boldsymbol{y} = \begin{pmatrix} x \\ y \\ p_1 \\ p_2 \end{pmatrix}, \tag{3.3}$$

and the vector field $\boldsymbol{f}$ for this system reads as

$$\boldsymbol{f}(\boldsymbol{y}) = \begin{pmatrix} p_1 \\ p_2 \\ n\, n_x \\ n\, n_y \end{pmatrix}, \tag{3.4}$$

where n_x and n_y are the partial derivatives of n. Observe that function $\boldsymbol{f}$ does not depend on s and therefore the system is said to be *autonomous*. The initial conditions are given by

$$\boldsymbol{y}_0 = \begin{pmatrix} x_0 \\ y_0 \\ p_{1,0} \\ p_{2,0} \end{pmatrix}, \tag{3.5}$$

Following up, we will describe the numerical methods for an autonomous system. We start with describing two basic Euler methods.

3.1 Basic Euler methods

Forward Euler
The first and most intuitive method is the *forward Euler* (FE) or Explicit Euler scheme, named after Leonhard Euler, who described it in 1768. The scheme is given by

$$\boldsymbol{y}_{i+1} = \boldsymbol{y}_i + h\,\boldsymbol{f}(\boldsymbol{y}_i), \qquad i = 0, 1, \ldots \tag{3.6}$$

Backward Euler
The second basic method is the *backward Euler* (BE) or implicit Euler scheme. The scheme is given by

$$\boldsymbol{y}_{i+1} = \boldsymbol{y}_i + h\,\boldsymbol{f}(\boldsymbol{y}_{i+1}), \qquad i = 0, 1, \ldots \tag{3.7}$$

which needs to be solved implicitly. Introducing the auxiliary vector $\boldsymbol{z} = \boldsymbol{y}_{i+1}$, the nonlinear system to solve at each integration step is then given by

$$\boldsymbol{F}(\boldsymbol{z}) = \boldsymbol{z} - h\boldsymbol{f}(\boldsymbol{z}) - \boldsymbol{y}_i = 0. \tag{3.8}$$

To approximate the zeros of $\boldsymbol{F}$, the Newton-Raphson method is used and reads

Initial guess:	$\boldsymbol{z}_0 = \boldsymbol{y}_i$,
For:	$k = 0, 1, 2, \ldots,$
Solve:	$\boldsymbol{J}(\boldsymbol{z}_k)\boldsymbol{s}_k = \boldsymbol{F}(\boldsymbol{z}_k)$,
Update:	$\boldsymbol{z}_{k+1} = \boldsymbol{z}_k - \boldsymbol{s}_k$,

where $\boldsymbol{J}$ is the Jacobi matrix of $\boldsymbol{F}$, defined as

$$\boldsymbol{J}(\boldsymbol{z}) = \boldsymbol{I} - h\frac{\partial \boldsymbol{f}}{\partial \boldsymbol{y}}(\boldsymbol{z}). \tag{3.9}$$

The stopping criterion used is $\|\boldsymbol{F}(\boldsymbol{z}_k)\|_2 \leq \delta$, for some tolerance δ. The tolerance is set to 10^{-6}.

3.2 Symplectic Euler methods

Another important class of methods are the symplectic methods, that preserve the Hamiltonian $\mathcal{H} = \mathcal{H}(\boldsymbol{q}, \boldsymbol{p})$ up to some order.

Symplectic Euler
For a general Hamiltonian system, the *symplectic Euler method* (SE) reads

$$\boldsymbol{p}_{i+1} = \boldsymbol{p}_i - h\frac{\partial \mathcal{H}}{\partial \boldsymbol{q}}(\boldsymbol{q}_i, \boldsymbol{p}_{i+1}), \tag{3.10a}$$

$$\boldsymbol{q}_{i+1} = \boldsymbol{q}_i + h\frac{\partial \mathcal{H}}{\partial \boldsymbol{p}}(\boldsymbol{q}_i, \boldsymbol{p}_{i+1}), \qquad i = 0, 1, \ldots \tag{3.10b}$$

Note that the variable $\boldsymbol{p}$ is taken implicitly and $\boldsymbol{q}$ explicitly, which can also be swapped. For a general separable Hamiltonian (2.9), the scheme reads

$$\boldsymbol{p}_{i+1} = \boldsymbol{p}_i - h\frac{\partial V}{\partial \boldsymbol{q}}(\boldsymbol{q}_i), \tag{3.11a}$$

$$\boldsymbol{q}_{i+1} = \boldsymbol{q}_i + h\frac{\partial T}{\partial \boldsymbol{p}}(\boldsymbol{p}_{i+1}), \qquad i = 0, 1, \ldots \tag{3.11b}$$

This can be solved explicitly, by first computing the value of $\boldsymbol{p}_{i+1}$. The explicit symplectic Euler scheme for Hamiltonian system (2.4) is given by

$$\boldsymbol{p}_{i+1} = \boldsymbol{p}_i + h\, n(\boldsymbol{q}_i)\, \nabla n(\boldsymbol{q}_i), \tag{3.12a}$$

$$\boldsymbol{q}_{i+1} = \boldsymbol{q}_i + h\, \boldsymbol{p}_{i+1}, \qquad i = 0, 1, \ldots \tag{3.12b}$$

Fourth-order symplectic Euler

A *fourth-order symplectic Euler scheme* (SE4) is considered by Yoshida [7]. Just like the previous method, the method considers the Hamiltonian system (2.4). The solution of this system can be given as

$$\boldsymbol{q}(\boldsymbol{q}_0, \boldsymbol{p}_0, \tau), \qquad \boldsymbol{p}(\boldsymbol{q}_0, \boldsymbol{p}_0, \tau), \tag{3.13}$$

where $\boldsymbol{q}_0$ and $\boldsymbol{p}_0$ are the initial conditions. The solution can also be considered as a symplectic map from the initial conditions to the state $\boldsymbol{q}(\tau)$, $\boldsymbol{p}(\tau)$. This map is denoted as $M(\tau)$. The idea is to approximate this map by a symplectic map $M_k(\tau)$, such that $M_k(\tau)$ approximates $M(\tau)$ to order τ^k.

The SE4 method uses this approximation for $k = 4$. In practice, this can be achieved in several ways. The method as described in [7] uses a procedure which is very similar to a Runge-Kutta integration step. Runge-Kutta methods will be described after this method. The method is similar to a Runge-Kutta method in the sense that the method constructs a sequence of maps with different coefficients.

The coefficients are chosen such that the Hamiltonian is conserved with an error of order h^4. These coefficients are given by the vectors $\boldsymbol{c} = (c_1, c_2, c_3, c_4)^T$ and $\boldsymbol{d} = (d_1, d_2, d_3, d_4)^T$ and have to satisfy 8 conditions, in order to ensure that the Hamiltonian is of order h^4. Two of those conditions are given by

$$\sum_{j=1}^{4} c_i = 1, \qquad \sum_{j=1}^{4} d_i = 1, \tag{3.14}$$

because the total step size should remain h. The other six complex conditions for $\boldsymbol{c}$ and $\boldsymbol{d}$ are given in a paper by Forest and Ruth [8]. They consider the following substitution for $\boldsymbol{c}$ and $\boldsymbol{d}$

$$\begin{aligned} c_1 &= x + \tfrac{1}{2}, & d_1 &= 2x + 1, \\ c_2 &= -x, & d_2 &= -4x - 1, \\ c_3 &= -x, & d_3 &= 2x + 1, \\ c_4 &= x + \tfrac{1}{2}, & d_4 &= 0, \end{aligned} \tag{3.15}$$

where x in this case is just an auxiliary variable. The common solution for the complex conditions is then given by the root of the polynomial

$$48x^3 + 24x^2 - 1 = 0 \tag{3.16}$$

This gives one real solution $x \approx 0.1756$. Substituting this result into the coefficients (3.15) gives the coefficients that are also used by Yoshida [7]

$$c_1 = c_4 = \frac{1}{2(2 - 2^{1/3})}, \qquad c_2 = c_3 = \frac{1 - 2^{1/3}}{2(2 - 2^{1/3})}, \tag{3.17a}$$

$$d_1 = d_3 = \frac{1}{2 - 2^{1/3}}, \qquad d_2 = -\frac{2^{1/3}}{2 - 2^{1/3}}, \qquad d_4 = 0. \tag{3.17b}$$

To get a feeling for the values of the coefficients, the values are given up to four decimals in Table 3.1.

c_1	0.6756	d_1	1.3512
c_2	-0.1756	d_2	-1.7024
c_3	-0.1756	d_3	1.3512
c_4	0.6756	d_4	0

Table 3.1: The values of the coefficients up to four decimals.

Table 3.1 shows that some of the coefficients are negative and the coefficients of $\boldsymbol{d}$ are in absolute value greater than 1. This causes problems when rays enter and leaves a lens. We will elaborate on this in the next chapter by use of an example.

Using coefficients $\boldsymbol{c}$ and $\boldsymbol{d}$, the method consists of 4 stages. At each iteration, introduce auxiliary vectors $\boldsymbol{z}_{1,0} = \boldsymbol{q}_i$ and $\boldsymbol{z}_{2,0} = \boldsymbol{p}_i$ to update the variables during the 4 stages. This implies that at the end of the iteration we find $\boldsymbol{q}_{i+1} = \boldsymbol{z}_{1,4}$ and $\boldsymbol{p}_{i+1} = \boldsymbol{z}_{2,4}$.

At each stage, the SE scheme (3.10) is applied to $\boldsymbol{z}_{1,j}$ and $\boldsymbol{z}_{2,j}$ from $j = 0$ to $j = 3$. The only difference is the step size within these stages. The step size of stage j is equal to $h\, c_j$ for the variables that are taken implicitly and $h\, d_j$ for the variables that are taken explicitly. The fourth-order symplectic Euler scheme reads as follows

$$
\begin{aligned}
&\text{Introduce:} && \boldsymbol{z}_{1,0} = \boldsymbol{q}_i, \\
& && \boldsymbol{z}_{2,0} = \boldsymbol{p}_i, \qquad i = 0, 1, \cdots \\
&\text{For:} && j = 0, 1, 2, 3, \\
&\text{Solve:} && \boldsymbol{z}_{1,j+1} = \boldsymbol{z}_{1,j} + h \cdot d_j \frac{\partial \mathcal{H}}{\partial \boldsymbol{p}}(\boldsymbol{z}_{1,j}, \boldsymbol{z}_{2,j+1}), \\
& && \boldsymbol{z}_{2,j+1} = \boldsymbol{z}_{2,j} - h \cdot c_j \frac{\partial \mathcal{H}}{\partial \boldsymbol{q}}(\boldsymbol{z}_{1,j}, \boldsymbol{z}_{2,j+1}), \\
&\text{Finally:} && \boldsymbol{q}_{i+1} = \boldsymbol{z}_{1,4}, \\
& && \boldsymbol{p}_{i+1} = \boldsymbol{z}_{2,4}.
\end{aligned}
\tag{3.18}
$$

As for the SE method, the SE4 scheme becomes explicit for a separable Hamiltonian.

The scheme for Hamiltonian (2.3) reads as

$$\begin{aligned}
&\text{Introduce:} && \boldsymbol{z}_{1,0} = \boldsymbol{q}_i, \\
& && \boldsymbol{z}_{2,0} = \boldsymbol{p}_i, \qquad i = 0, 1, \cdots \\
&\text{For:} && j = 0, 1, 2, 3, \\
&\text{Solve:} && \boldsymbol{z}_{2,j+1} = \boldsymbol{z}_{2,j} + h \cdot c_j \cdot n(\boldsymbol{z}_{1,j}) \cdot \nabla n(\boldsymbol{z}_{1,j}), \\
& && \boldsymbol{z}_{1,j+1} = \boldsymbol{z}_{1,j} + h \cdot d_j \cdot \boldsymbol{z}_{2,j+1}, \\
&\text{Finally:} && \boldsymbol{q}_{i+1} = \boldsymbol{z}_{1,4}, \\
& && \boldsymbol{p}_{i+1} = \boldsymbol{z}_{2,4}.
\end{aligned} \tag{3.19}$$

3.3 Runge-Kutta method

A different class of methods is referred to as the *Runge-Kutta* methods, named after the German mathematicians Carl Runge and Wilhelm Kutta, who first described and analysed the methods around 1900.

Explicit 4-stage Runge-Kutta
The most widely used Runge-Kutta method is the *explicit 4-stage Runge-Kutta* (RK4) method. The scheme is given by

$$\begin{aligned}
&\boldsymbol{k}_1 = \boldsymbol{f}(\boldsymbol{y}_i), \\
&\boldsymbol{k}_2 = \boldsymbol{f}(\boldsymbol{y}_i + \tfrac{1}{2}h\boldsymbol{k}_1), \\
&\boldsymbol{k}_3 = \boldsymbol{f}(\boldsymbol{y}_i + \tfrac{1}{2}h\boldsymbol{k}_2), \\
&\boldsymbol{k}_4 = \boldsymbol{f}(\boldsymbol{y}_i + h\boldsymbol{k}_3), \\
&\boldsymbol{y}_{n+1} = \boldsymbol{y}_n + \tfrac{1}{6}h(\boldsymbol{k}_1 + 2\boldsymbol{k}_2 + 2\boldsymbol{k}_3 + \boldsymbol{k}_4), \qquad i = 0, 1, \cdots
\end{aligned} \tag{3.20}$$

3.4 Gauss-Legendre method

Fourth-order Gauss-Legendre
The *fourth-order Gauss-Legendre* (GL4) method is an implicit method. The scheme is given by

$$\boldsymbol{k}_1 = \boldsymbol{f}\left(\boldsymbol{y}_i + h(\tfrac{1}{4}\boldsymbol{k}_1 + (\tfrac{1}{4} - \tfrac{1}{2\sqrt{3}})\boldsymbol{k}_2)\right), \tag{3.21a}$$

$$\boldsymbol{k}_2 = \boldsymbol{f}\left(\boldsymbol{y}_i + h((\tfrac{1}{4} + \tfrac{1}{2\sqrt{3}})\boldsymbol{k}_1 + \tfrac{1}{4}\boldsymbol{k}_2)\right), \tag{3.21b}$$

$$\boldsymbol{y}_{n+1} = \boldsymbol{y}_n + \tfrac{1}{2}h(\boldsymbol{k}_1 + \boldsymbol{k}_2), \qquad i = 0, 1, \cdots \tag{3.21c}$$

Observe that the vectors $\boldsymbol{k}_1$ and $\boldsymbol{k}_2$ have to be solved simultaneously, which makes this an implicit method. The procedure is similar to the Backward Euler scheme. Introduce auxiliary vectors $\boldsymbol{z}_1$ and $\boldsymbol{z}_2$ as

$$\boldsymbol{z}_1 = \boldsymbol{y}_i + h(\tfrac{1}{4}\boldsymbol{k}_1 + (\tfrac{1}{4} - \tfrac{1}{2\sqrt{3}})\boldsymbol{k}_2) \tag{3.22a}$$

$$\boldsymbol{z}_2 = \boldsymbol{y}_i + h((\tfrac{1}{4} + \tfrac{1}{2\sqrt{3}})\boldsymbol{k}_1 + \tfrac{1}{4}\boldsymbol{k}_2) \tag{3.22b}$$

Notice that the system of equations (3.21a) and (3.21b) can then be written as

$$\boldsymbol{F}(\boldsymbol{k}) = \begin{pmatrix} \boldsymbol{k}_1 - \boldsymbol{f}(\boldsymbol{z}_1) \\ \boldsymbol{k}_2 - \boldsymbol{f}(\boldsymbol{z}_2) \end{pmatrix} = 0, \qquad \boldsymbol{k} = \begin{pmatrix} \boldsymbol{k}_1 \\ \boldsymbol{k}_2 \end{pmatrix}, \tag{3.23}$$

The remaining task is to find or approximate the zeros of $\boldsymbol{F}(\boldsymbol{k})$. The Newton-Raphson method is used to approximate the roots. The procedure is given by

$$\begin{aligned} &\text{Initial guess:} && \boldsymbol{k}_0 = \begin{pmatrix} \boldsymbol{f}(\boldsymbol{y}_n) \\ \boldsymbol{f}(\boldsymbol{y}_n) \end{pmatrix}, \\ &\text{For:} && l = 0, 1, 2, \ldots, \\ &\text{Solve:} && \boldsymbol{J}(\boldsymbol{k}_l)\boldsymbol{s}_l = \boldsymbol{F}(\boldsymbol{k}_l), \\ &\text{Update:} && \boldsymbol{k}_{l+1} = \boldsymbol{k}_l - \boldsymbol{s}_l, \end{aligned}$$

where $\boldsymbol{J}(\boldsymbol{k})$ is the Jacobi matrix of $\boldsymbol{F}(\boldsymbol{k})$, defined as

$$\boldsymbol{J}(\boldsymbol{k}) = \begin{pmatrix} \boldsymbol{I} - h\frac{1}{4}\frac{\partial \boldsymbol{f}}{\partial \boldsymbol{y}}(\boldsymbol{z}_1) & -h(\frac{1}{4} - \frac{1}{2\sqrt{3}})\frac{\partial \boldsymbol{f}}{\partial \boldsymbol{y}}(\boldsymbol{z}_1) \\ -h(\frac{1}{4} + \frac{1}{2\sqrt{3}})\frac{\partial \boldsymbol{f}}{\partial \boldsymbol{y}}(\boldsymbol{z}_2) & \boldsymbol{I} - h\frac{1}{4}\frac{\partial \boldsymbol{f}}{\partial \boldsymbol{y}}(\boldsymbol{z}_2) \end{pmatrix}. \tag{3.24}$$

The stopping criterion used is $\|\boldsymbol{F}(\boldsymbol{k}_l)\| \leq \delta$, for tolerance δ.

Chapter 4

GRIN lenses

To verify that we can simulate rays with the ODE systems of Chapter 1 and 2, using the time-integration methods of Chapter 3, the following optical lenses are considered: the Luneburg lens, the Maxwell fish-eye lens and a gradient-index lens with cylindrical symmetry. All these lenses have in common that they belong to the family of *gradient-index lenses*, i.e., GRIN lenses. GRIN lenses change the path of light due to a gradient in the refractive index of the material. Figure 4.1 shows an example of how GRIN lenses change the path of a light ray.

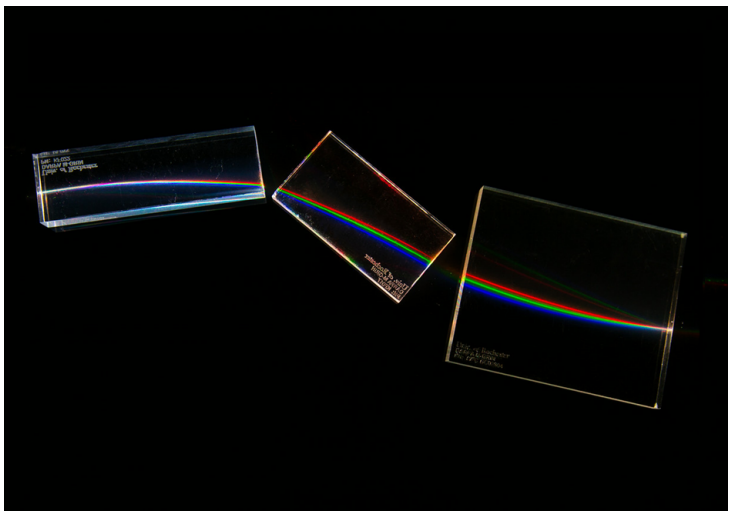

Figure 4.1: Gradient-index lenses and their effect on light rays.

The lenses can be mathematically described by their corresponding refractive index function $n = n(\boldsymbol{q})$, as function of the position $\boldsymbol{q}$. We consider cross-sections of the lenses, to reduce the complexity of the problem. This is done by considering the lens in a plane, e.g. $z = 0$. The light rays are also chosen to propagate in this plane at all times by choosing proper initial conditions. Next, we describe the individual lenses in more detail.

4.1 Luneburg lens

The first lens is the *Luneburg lens*, which was proposed by Rudolf Luneburg in 1944. The Luneburg lens is a lens with spherical symmetry. The lens that we will describe can be considered as an ideal Luneburg lens, where the gradient of the refractive index is a continuous function. In practice, such a lens is often approximated by creating discrete layers using, for example, 3D-printing techniques. An example of such a 3D-printed Luneburg lens can be seen in Figure 4.2. The smallest Luneburg lens that works for visible light is about 15 μm in diameter [9]. This Luneburg lens is created using the *subsurface controllable refractive index via beam exposure* (SCRIBE) method. More details and results of this method are described in paper [9].

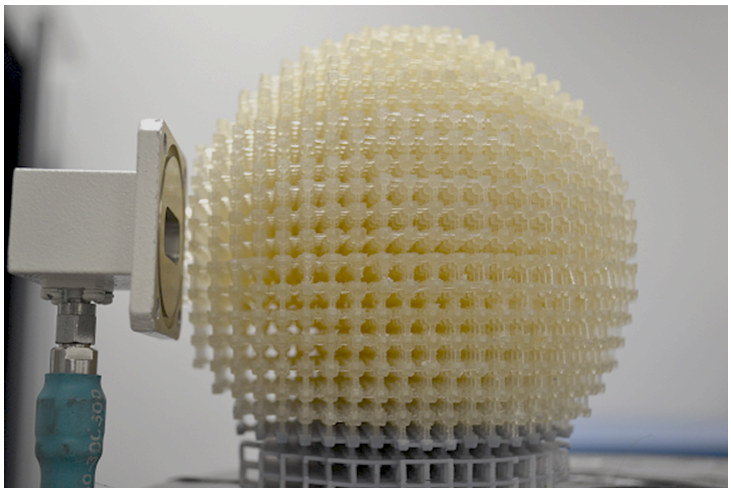

Figure 4.2: A 3D-printed Luneburg lens consisting of discrete layers. The layers are more dense towards the centre of the lens to create a higher refractive index.

The Luneburg lens has the property that it can focus any incoming plane wave. The focus is created on the opposite side of the lens. The reverse optical effect is also possible, because the lens can convert a point source on the edge of the lens to a plane wave leaving the lens. Both cases will be simulated as verification.

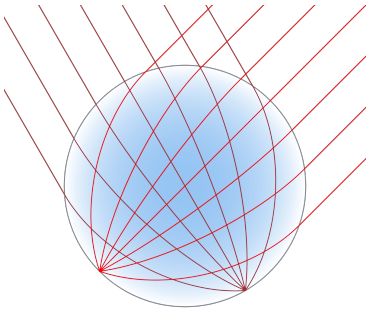

Figure 4.3: Cross-section of an ideal Luneburg lens. The figure also illustrates how rays are focused on the edge.

We will consider the cross-section of the lens in the plane $z = 0$. A sketch of this cross-section can be seen in Figure (4.3). Due to spherical symmetry, the refractive index

only changes as function of the radius r to the centre of the lens. Therefore, it makes sense to place the centre of the lens in the origin. The refractive index function of an ideal Luneburg lens is described by

$$n(r) = \begin{cases} n_0\sqrt{2 - \left(\frac{r}{R}\right)^2}, & r \leq R, \\ n_0, & r > R. \end{cases} \tag{4.1}$$

where n_0 is the refractive index of the surrounding medium and R is the radius of the lens. Observe that the refractive index varies from $n_0\sqrt{2}$ at the core of the lens to n_0 at the edge of the lens. The parameters for the lens are chosen as $n_0 = 1$, representing vacuum, and $R = 1$ mm.

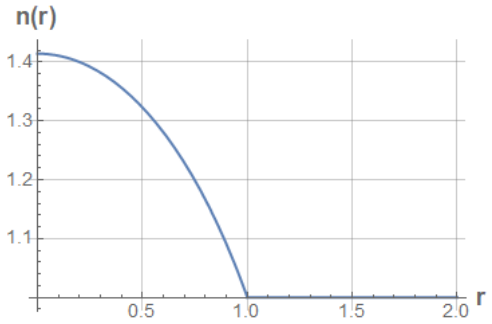

Figure 4.4: The refractive index for the Luneburg lens.

The refractive index for a perfect Luneburg lens is plotted in Figure 4.4. This verifies that function (4.1) is continuous. This is important, because it tells us that there is no refraction at the boundary $r = R$. Moreover, we observe that the derivative is not a continuous function. Later, we will verify that the gradient of n accounts for the refraction of a light ray. For spherical symmetric lenses, the gradient of n is simply given by

$$\nabla n = n'(r)\,\hat{\mathbf{e}}_r, \tag{4.2}$$

where the derivative of $n(r)$ is given by

$$n'(r) = \begin{cases} -\dfrac{n_0\, r}{R^2\sqrt{2 - \left(\frac{r}{R}\right)^2}}, & r \leq R, \\ 0, & r > R. \end{cases} \tag{4.3}$$

The derivative of n is plotted in figure 4.5. A direct result of Snell's law for continuously varying media is that a higher value of $|n'(r)|$ implies more refraction. Figure 4.5 therefore indicates that rays refract more towards the edge of the lens.

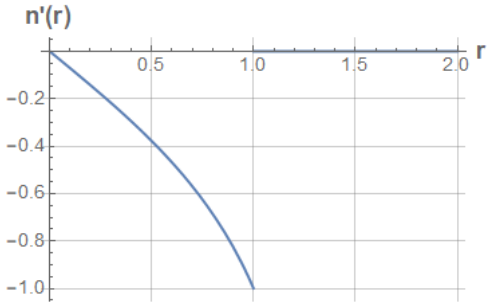

Figure 4.5: The derivative of the refractive index of the Luneburg lens.

4.2 Maxwell's fish-eye lens

The next lens is called *Maxwell's fish-eye lens*, described by James Clerk Maxwell in 1854. Also this lens is spherical. The most interesting optical effect of this lens is that any point source on the edge is focused on the opposite side of the sphere. All rays originating from such a point source on the edge will have the same optical path length within the lens, because they enter and leave the lens at the same point. Otherwise, it would not correspond with Fermat's principle, described in Chapter 1. A sketch of a cross-section of this lens is given in Figure 4.6.

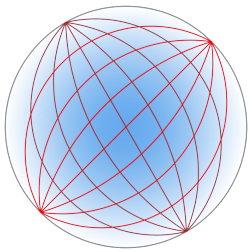

Figure 4.6: Cross-section of Maxwell's fish-eye lens. It illustrates how a point source of the edge is focused on the opposite side of the lens.

The refractive index function $n(x, y)$ of Maxwell's fish-eye lens is described by

$$n(r) = \begin{cases} \dfrac{2n_0}{1 + \left(\frac{r}{R}\right)^2}, & r \leq R, \\ n_0, & r > R, \end{cases} \tag{4.4}$$

where all parameters are defined as for the Luneburg lens. Note that the refractive index for this lens varies from $2n_0$ at the core of the lens to n_0 at the edge. A plot for the refractive index can be seen in Figure 4.7.

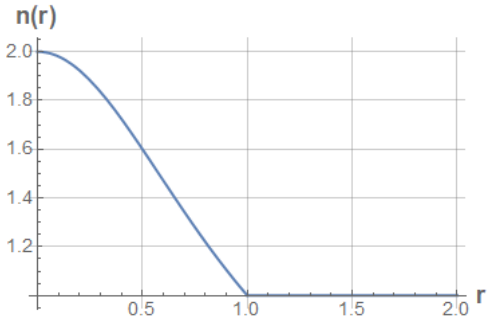

Figure 4.7: The refractive index of Maxwell's fish-eye lens.

The derivative of n for this lens reads as

$$n'(r) = \begin{cases} -\dfrac{-4\,n_0\,r}{R^2\left(1+\left(\frac{r}{R}\right)^2\right)^2}, & r \leq R, \\ 0, & r > R. \end{cases} \tag{4.5}$$

A plot of $n'(r)$ can be seen in Figure 4.8. We observe that $|n'(r)|$ inside the lens, i.e. for $0 < r < 1$, is strictly less compared to the Luneburg lens, seen in figure 4.5. Therefore, we expect more refraction for rays inside the Maxwell's fish eye lens compared to the Luneburg lens. If we compare the sketch of Maxwell's fish eye lens in Figure 4.6 with the sketch of the Luneburg lens in Figure 4.3, this holds.

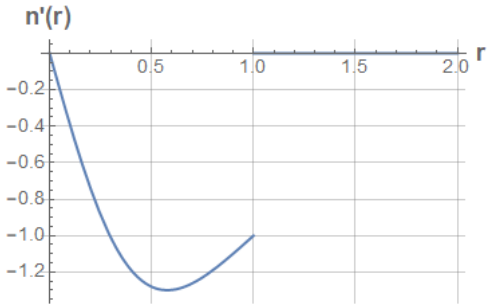

Figure 4.8: The derivative of the refractive index of Maxwell's fish-eye lens.

4.3 Cylindrical GRIN lens

The third lens is a *gradient-index lens with cylindrical symmetry* [10]. The lens is taken as a cylinder with length L and radius R. For this lens, r is defined to be the radial distance from the symmetric axis. The refractive index only changes as a function of r. Again, we consider a cross-section of the lens by considering the plane $z = 0$. The cross-section is taken over the length of the cylinder, giving a rectangle with dimensions $L \times 2R$. The x-axis is taken as the axis of symmetry, which means the cylinder can be taken from $x = 0$ to $x = L$. A drawing of this type of GRIN lens is given in Figure 4.9.

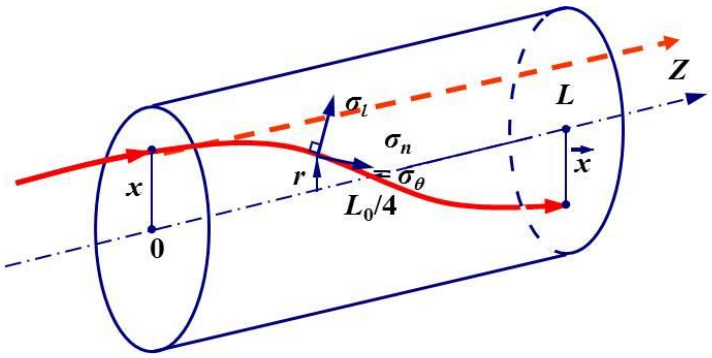

Figure 4.9: Sketch of a gradient-index lens with cylindrical symmetry. The sinusoidal behaviour of the rays inside the lens is also shown here.

We have that the radial distance r is equal to the absolute value of y. The lens has the special property that rays will follow sinusoidal trajectories. The lens is generally used to focus parallel beams.

The refractive index function n is described by

$$n(r) = \begin{cases} n_1\sqrt{1-(Ar)^2}, & r \leq R, \\ n_0, & r > R, \end{cases} \tag{4.6}$$

where n_0 is again the refractive index of the surrounding medium, R is the radius of the cylinder and A is a positive constant. Parameter n_1 is defined to be the refractive index at the core of the cylinder, which are in this case points inside the lens on the symmetric axis $z = 0$. All parameters n_1, A and R can be chosen as part of the manufacturing process. Important is that the refractive index varies between n_1 at the core of the cylinder to $n_1\sqrt{1-A^2}$ at the edge. A plot of the refractive index for the parameters $n_1 = 1.5, A = 0.5, R = 1$ and $n_0 = 1$ is given in figure 4.10.

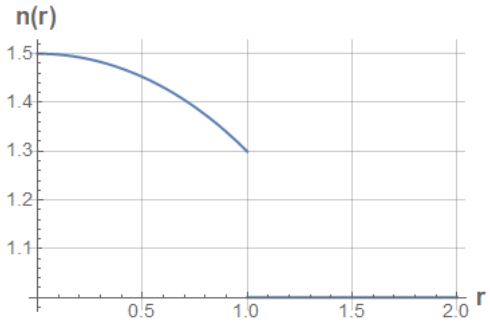

Figure 4.10: The refractive index of the cylindrical GRIN lens.

The derivative of n reads

$$n'(r) = \begin{cases} -\dfrac{A^2\, n_1\, r}{\sqrt{1-(Ar)^2}}, & r \leq R, \\ 0, & r > R. \end{cases} \tag{4.7}$$

A plot of the derivative can be seen in figure 4.11.

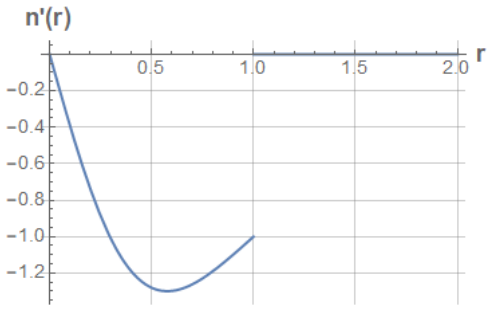

Figure 4.11: The derivative of the refractive index of the cylindrical GRIN lens.

This lens differs from the other two lenses in the sense that the refractive index function is not necessarily continuous, which is clear from Figure 4.10. The result of this is that *refraction* occurs at the edge of the lens. Refraction occurs when light enters a medium with a different refractive index and the result of it is that the light bends. The angle of refraction is described by Snell's law, given by

$$n_1 \sin\theta_1 = n_2 \sin\theta_2, \tag{4.8}$$

where in this case light travels from medium with refractive index n_1 to a medium with index n_2. Therefore, θ_1 is the angle of incidence and θ_2 is the angle of refraction. Figure 4.12 illustrates Snell's law in more detail. Observe that the *interface* in Figure 4.12 is in our case the edge of the lens.

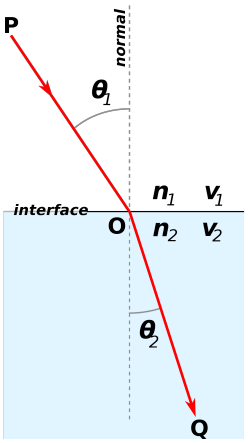

Figure 4.12: Light enters a medium with a higher refractive index ($n_2 > n_1$). Refraction occurs, which means that the light bends.

If a ray inside the lens approaches the edge of the lens with an angle of incidence θ_1 greater or equal than the *critical angle* θ_{crit}, *total internal reflection* occurs. Total internal reflection simply means that the ray stays inside the lens, because the angle θ_2 is greater or equal than 90°. Therefore, the critical angle can be calculated as

$$n_1 \sin \theta_{\text{crit}} = n_2, \qquad n_1 > n_2, \tag{4.9}$$

or equivalently,

$$\theta_{\text{crit}} = \arcsin \frac{n_2}{n_1}, \qquad n_1 > n_2. \tag{4.10}$$

Refraction and total internal reflection could be avoided at the edges $r = R$ by choosing the parameter A in a special way. We choose A such that $n = n(r)$ becomes a continuous function, i.e., by requiring $n(R) = n_0$. This gives a constraint on the parameter A and reads

$$A = \frac{1}{R}\sqrt{1 - \left(\frac{n_0}{n_1}\right)^2}. \tag{4.11}$$

If we substitute the equation for parameter A (4.11) with $n_1 = \sqrt{2}n_0$ into the refractive index function of the cylindrical GRIN lens (4.6), we obtain the refractive index function of the Luneburg lens (4.1). This shows how close the different lenses actually are. Next, we describe the starting conditions for the light rays for the various lenses.

Scenario A
The first scenario is where rays start at a point on the edge of the lens. The variables used for that are given in the tables below.

Variable	Value	Description
x_0	-R	Initial x-value
y_0	0	Initial y-value
α	$(-\frac{\pi}{2}, \frac{\pi}{2})$	Initial angle between the direction vector and the positive x-axis
$p_{1,0}$	$\cos\alpha$	Initial p_1-value
$p_{2,0}$	$\sin\alpha$	Initial p_2-value

Table 4.1: Starting conditions for rays entering the Luneburg and Maxwell fish-eye lens

Variable	Value	Description
x_0	0	Initial x-value
y_0	0	Initial y-value
α	$(-\frac{\pi}{6}, \frac{\pi}{6})$	Initial angle between the direction vector and the positive x-axis
$p_{1,0}$	$\cos\alpha$	Initial p_1-value
$p_{2,0}$	$\sin\alpha$	Initial p_2-value

Table 4.2: Starting conditions for rays entering the cylindrical GRIN lens

Scenario B
In the second scenario, the light starts as a plane wave. We consider a plane wave which is parallel to the y-axis. To simulate a plane wave, the initial y-values of the rays are varied, while the initial angle α is set to zero. The variables are given in the tables below.

Variable	Value
x_0	-2
y_0	$(-R, R)$
α	0
$p_{1,0}$	$\cos\alpha$
$p_{2,0}$	$\sin\alpha$

Table 4.3: Starting conditions for rays entering the Luneburg and Maxwell fish-eye lens

Variable	Value
x_0	0
y_0	$(-R, R)$
α	0
$p_{1,0}$	$\cos\alpha$
$p_{2,0}$	$\sin\alpha$

Table 4.4: Starting conditions for rays entering the cylindrical GRIN lens

Chapter 5

Numerical simulations

In this chapter, rays and wavefronts will be simulated through various lenses from Chapter 4. To numerically approximate the rays and wavefronts, the time integration methods of chapter 3 are applied to the characteristic systems of chapter 1. When symplectic methods are used, the Hamiltonian system from chapter 2 is used instead. The numerical results were obtained using the software Matlab.

5.1 Numerical results

Luneburg lens

We start with presenting the numerical results for the Luneburg lens. Parameters for the simulation are the step-size h, the number of steps N, the number of simulated rays N_r and the number of simulated wavefronts N_w. The two plots in Figure 5.1 show the numerical results for this set of parameters.

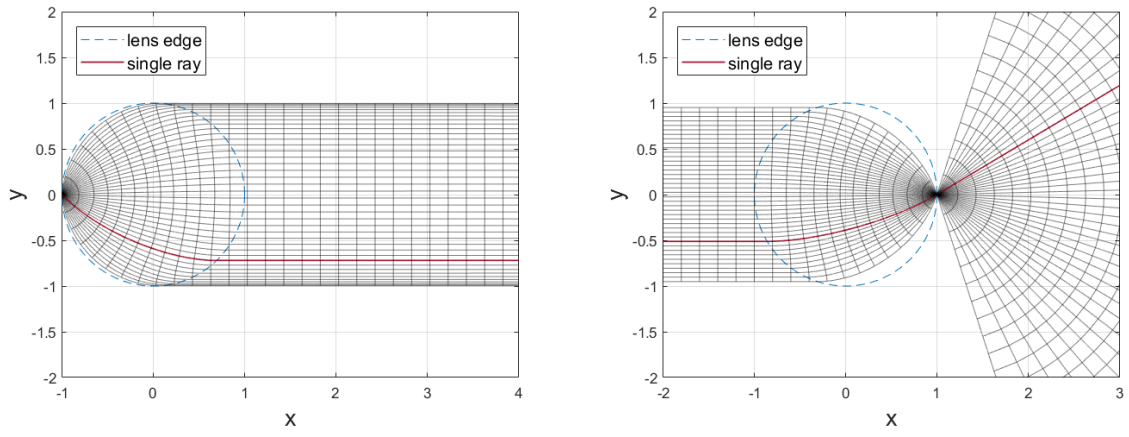

(a) Scenario A (b) Scenario B

Figure 5.1: Rays and wavefronts in the Luneburg lens, using the Gauss-Legendre method with $h = 10^{-3}$, $N = 10^4$, $N_r = 40$ and $N_w = 50$. The unit of x and y is mm.

In Figure 5.1, it can be observed that the optical effects of the Luneburg lens can be perfectly simulated by use of a proper method and suitable parameters. Both the rays and

wavefronts are shown and they seem to verify the fact that they should be perpendicular. Both plots in Figure 5.1 also confirm the properties of the Luneburg lens. Figure 5.1a confirms that the lens is able to convert a point source on the edge to a plane wave outside the lens. In particular, this plane wave has height $2R$. On the other hand, Figure 5.1b confirms that the lens is capable of focusing a plane wave on its edge. Due to the spherical symmetry of the lens, any desired finite height plane wave can be created or focused by choosing R accordingly. The plots in Figure 5.1 also both confirm that there is no refraction when the rays leave the lens, as described in the previous section.

Maxwell's fish-eye lens

Next, we present the numerical results of the Maxwell fish-eye lens. Figure 5.2 contains the numerical results for the two scenarios.

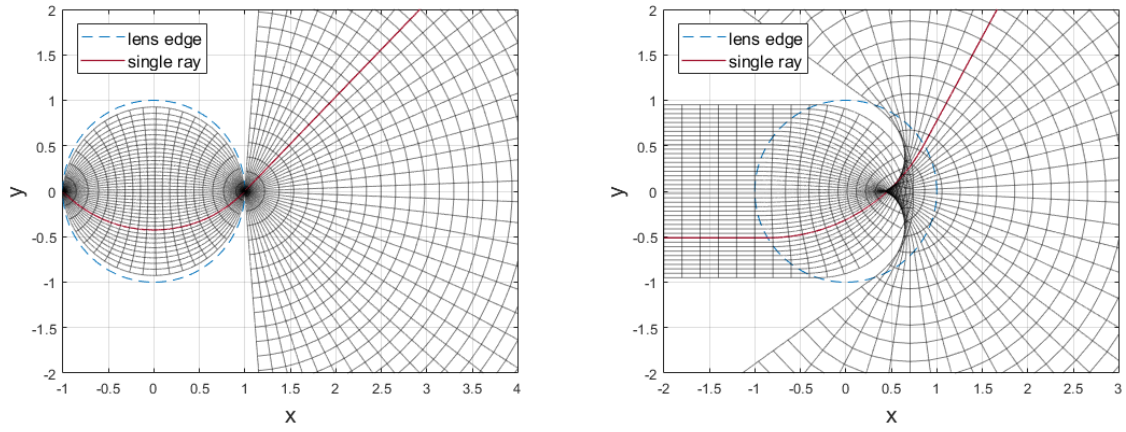

(a) Scenario A

(b) Scenario B

Figure 5.2: Rays and wavefronts in the Maxwell fish-eye lens, using the Gauss-Legendre method with $h = 10^{-3}$, $N = 10^4$, $N_r = 40$ and $N_w = 50$. The unit of x and y is mm.

Figure 5.2a verifies the symmetric optical effect that occurs when a point source is placed on the edge of the lens, i.e., the rays are symmetrically focused on the opposite side of the lens. It also seems as if the rays inside the lens follow a circular trajectory. On the other hand, Figure 5.2b shows a more chaotic pattern. The chaotic pattern in the middle of the figure can be explained by the bending rays that do not focus in one point like in Figure 5.2a. Remarkably, the outer starting rays almost make a full turn within the lens. Comparing the plots in Figure 5.2 and 5.1 verifies that rays refract more in the Maxwell fish-eye lens, just as described in Chapter 4.

Cylindrical GRIN lens

Lastly, we present the numerical results of the GRIN lens with cylindrical symmetry, for which we assume a length $L = 10$ mm. Furthermore, we choose the parameters such that the refractive index function coincides with the refractive index function of the Luneburg lens with $R = 1$ mm and $n_0 = 1$. Using the results from Chapter 4, the remaining parameters are taken as $n_1 = \sqrt{2}n_0$ and $A = \frac{1}{\sqrt{2}}$ mm^{-1}. The plots in Figure 5.3 show the numerical results.

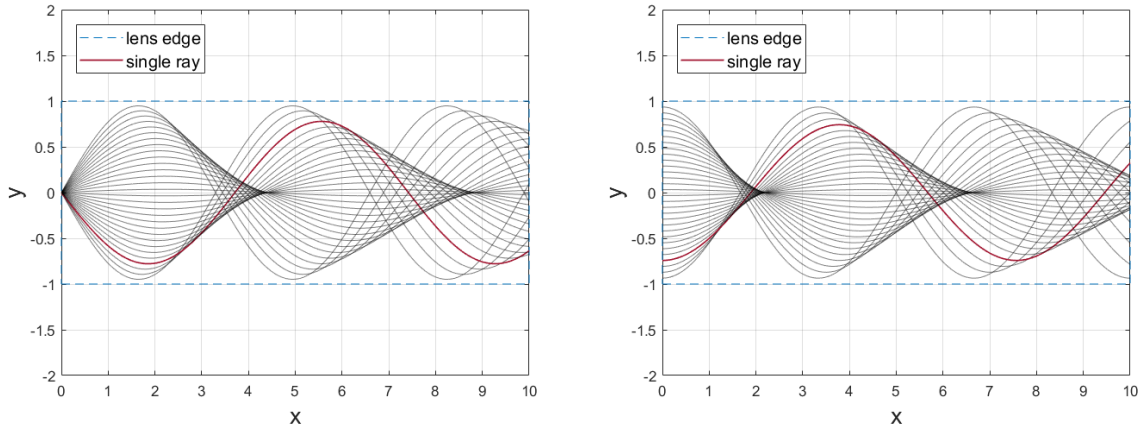

(a) Scenario A (b) Scenario B

Figure 5.3: Rays in the cylindrical GRIN lens, using the Gauss-Legendre method with $h = 5 \times 10^{-3}$, $N = 5 \times 10^3$ and $N_r = 30$. Parameter $A \approx 0.71$ mm^{-1}. The unit of x and y is mm.

Both plots in Figure 5.3 confirm the sinusoidal behaviour of the rays. The only real difference is that in Figure 5.3a the rays start at a zero of the sinusoidal function, while in Figure 5.3b the rays start at an extreme value. Remarkably, the sinusoidal functions do not have the same period, in particular, there seems to be an inverse relation between the amplitude and the period of a ray. This explains why there is no focus in the lens and why it seems as if this focus becomes worse over the length of the lens L. This lack of focus is called *aberration* in Optics. The aberration for this lens can be significantly reduced by choosing a different A parameter. The numerical result for scenario B with $A = 0.20$ is given in Figure 5.4. In this case, the wavefronts are plotted because the aberration is small enough.

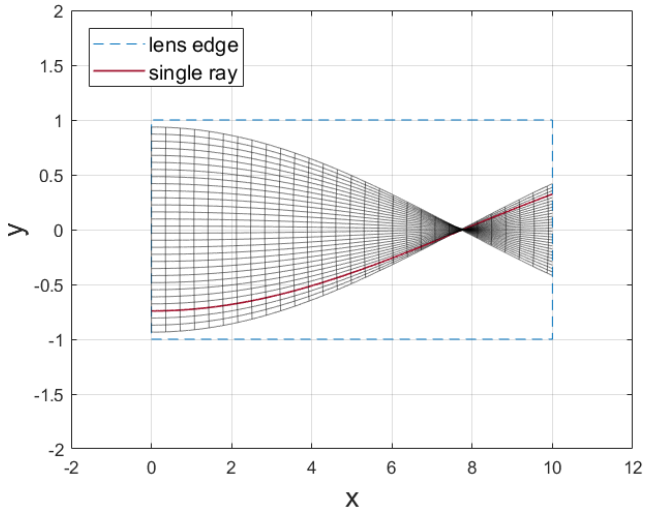

Figure 5.4: Rays and wavefronts in the cylindrical GRIN lens for scenario B, using the Gauss-Legendre method with $A = 0.20$ mm^{-1}. The unit of x and y is mm.

Observe that in Figure 5.4, rays are only plotted inside the lens. The reason for that is that refraction occurs for this lens on the right side, where rays generally do not leave

the lens perpendicular to the lens edge. The simulation of refraction is outside the scope of this report. To give an idea, Figure 5.5 shows what refraction at the lens edge for a cylindrical GRIN lens looks like [11].

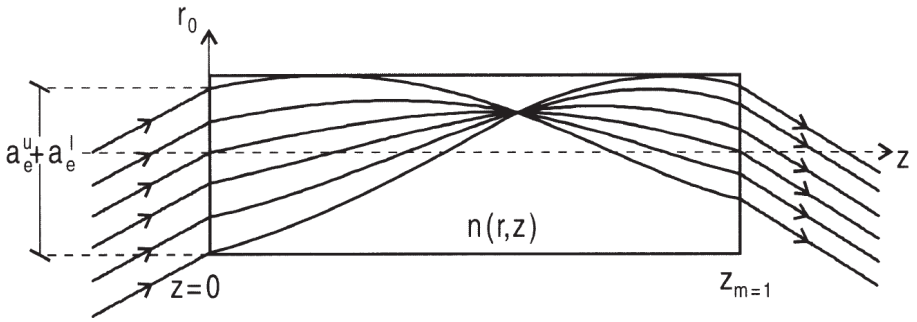

Figure 5.5: Refraction at both ends for a cylindrical GRIN lens.

A good question at this point is: how does the aberration change for this lens. Also, could the refractive index function (4.6) be modified such that this aberration does not occur at all? To answer the first question, we will use a result of a paper by Hiroshi Ohno [10]. In this paper an analytical solution is given for rays in this specific cylindrical GRIN lens, described by the refractive index (4.6). In this analytical solution, a period Λ occurs and is given by

$$\Lambda = \frac{2\pi}{A}\sqrt{1-(A\,y_0)^2}. \tag{5.1}$$

Observe that the period Λ depends on the fixed parameter A and the amplitude y_0. A plot of Λ versus y_0 for the rays of Figure 5.4 is given in Figure 5.6.

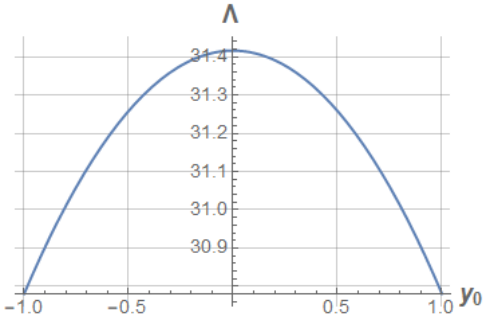

Figure 5.6: The period of a ray Λ (in mm) versus the initial y-value (in mm) of a ray in scenario B for the cylindrical GRIN lens. A ≈ 0.71.

The parameter Λ enables us to quantify the aberration, by looking at the maximum difference in period between the rays, which we refer to as $\Delta\Lambda$. From Figure 5.6 it is clear that the maximum period is attained at $y_0 = 0$ and the minimum period occurs at the lens edges, i.e., where $y_0 = \pm R$. Hence, $\Delta\Lambda$ is given by

$$\Delta\Lambda = \frac{2\pi}{A}(1-\sqrt{1-A^2R^2}). \tag{5.2}$$

For the lens in Figure 5.4 we have $\Delta\Lambda \approx 0.63$ mm. We can interpret this as the horizontal aberration after exactly one period. Observe that the focus in Figure 5.4 occurs after

a quarter of the period. Therefore, the aberration at that point can be quantified as $\Delta\Lambda/4 \approx 0.16$ mm. Similarly, we can quantify the aberration for the lens in Figure 5.3b. For that lens, we have $\Delta\Lambda \approx 2.60$ mm. Hence, the quantified aberration at the second focus, which occurs after 3/4-period, can be quantified as approximately 1.95 mm. It seems that the focus stretches from $z = 5$ to $z = 7$ which agrees with this result.

Next, we consider the other question: Is there a refractive index function like (4.6), that is free of aberration inside the lens. In fact, the hyperbolic secant (HS) function is the key in solving this problem. The refractive index function n for this cylindrical lens is given by [12]

$$n(y) = \begin{cases} n_1 \operatorname{sech}(Ay), & r \leq R, \\ n_0, & r > R, \end{cases} \tag{5.3}$$

where all variables are defined as before. The hyperbolic secant function is given by

$$\operatorname{sech}(x) = \frac{1}{\cosh x} = \frac{2}{e^x + e^{-x}}. \tag{5.4}$$

We refer to this kind of lens as a cylindrical HS-GRIN lens. Without going into further detail of this particular lens, we simulate the lens to verify the result. We consider the parameters as in Figure 5.3b, because aberration is very apparent there. The results are shown in Figure 5.7. The rays in Figure 5.7 seem to focus perfectly.

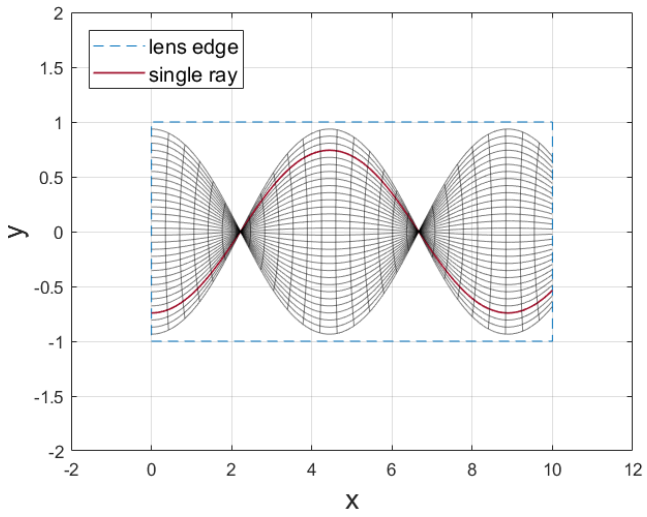

Figure 5.7: Rays and wavefronts in the cylindrical HS-GRIN lens for scenario B, using the Gauss-Legendre method with parameters similar to Figure 5.3b and $N_w = 50$. The unit of x and y is mm.

5.2 Error comparison

In this section, we will discuss how well the various numerical methods perform for the three gradient-index lenses. The following methods will be compared: forward Euler (FE), symplectic Euler (SE), fourth-order symplectic Euler (SE4), explicit 4-stage Runge-Kutta (RK4) and fourth-order Gauss-Legendre (GL4). What first comes to mind is comparing the methods with respect to the analytical solution of the ray equation (1.19), describing a single ray. However, finding such a solution can be very hard. Therefore, we also consider an easier approach, by using the Hamiltonian.

The derivations of these analytical solutions is outside the scope of this report. However, we can perform an error comparison by using the analytical solutions presented by Hiroshi Ohno [10]. In this paper, the analytical solutions are given for the perfect Luneburg lens and the cylindrical GRIN-lens that we described. These analytical solutions can be found by integrating the ray equation (1.19) for the refractive index function for the lens at hand.

Luneburg lens
For the Luneburg lens, we consider a ray parallel to the x-axis that starts at the edge of the lens. The analytical solution for this ray is given by [10]

$$\left(\frac{y}{y_0}\right)^2 + \left(\frac{x}{R} + \sqrt{1 - \left(\frac{y_0}{R}\right)^2}\frac{y}{y_0}\right)^2 = 1. \tag{5.5}$$

This is an elliptic curve and can be rewritten as

$$x = R\left(\pm\sqrt{1 - \left(\frac{y}{y_0}\right)^2} - \sqrt{1 - \left(\frac{y_0}{R}\right)^2}\frac{y}{y_0}\right). \tag{5.6}$$

As example, we assume that the ray enters the upper half of the lens from the left, i.e., $y_0 > 0$ and $x_0 < 0$. Because the ray starts exactly at the edge, a circle, we have

$$x_0^2 + y_0^2 = 1. \tag{5.7}$$

By choosing y_0 in (-R,R), the value of x_0 can be calculated as

$$x_0 = -\sqrt{1 - y_0^2}. \tag{5.8}$$

The exact solution under these assumptions is given by (5.6) with the plus sign, where y is taken from 0 to y_0. The exact ray is shown in Figure 5.8, together with some numerical methods. RK4 and GL4 are not shown here because they cannot be distinguished on this level with the SE4 method.

An importation remark here, is that the SE4 method is being slightly modified from this point. As described in Chapter 3, SE4 consists of 4 stages with different coefficients. Because some coefficients are rather big and negative, the method fails when the ray is close to the edge of the lens, with respect to the step size h. Therefore, the GL4 method is used instead when the method gets outside the lens during the 4 stages of the method, which may happen although the iteration starts and ends inside the lens.

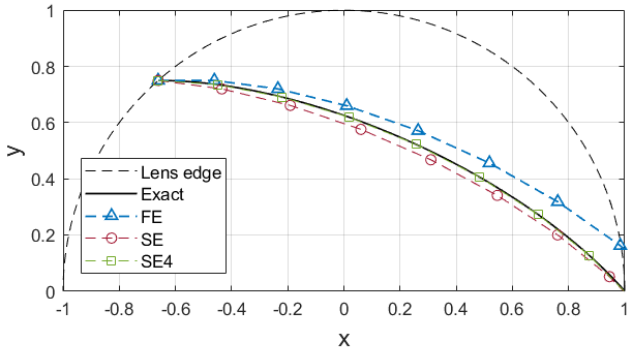

Figure 5.8: Several numerical methods and the exact solution for the Luneburg lens. $h = 0.2$, $y_0 = 0.75$, $R = 1$ and $n_0 = 1$.

Next, we like to perform an error comparison using the exact ray solution $x = x(y)$, given by (5.6). We define the error ε_1 as

$$\varepsilon_1 = \max |x_i - x(y_i)|, \tag{5.9}$$

for all (x_i, y_i) that are inside the lens. The error ε_1 can be computed as function of the step-size h. This can be done for each numerical time integration method. The results for a ray as in Figure 5.8 are given in Figure 5.9.

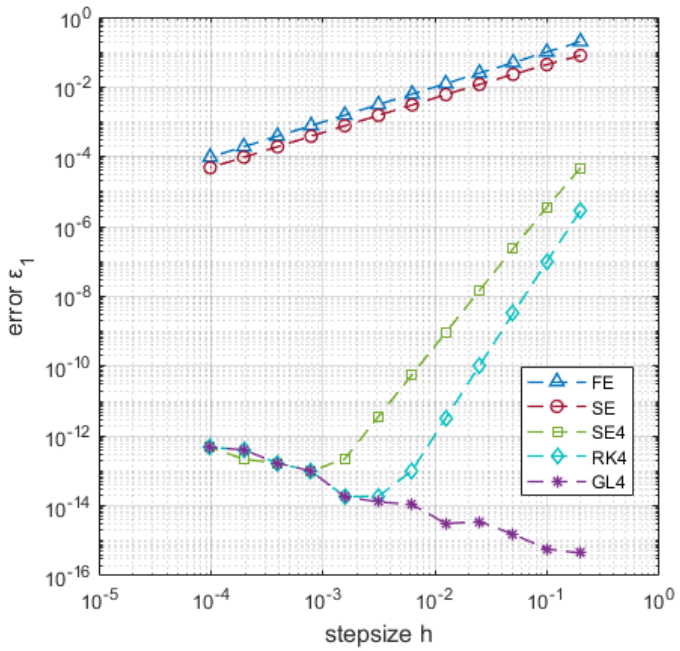

Figure 5.9: Error comparison for a ray starting on the edge of the Luneburg lens.

Figure 5.9 shows that the error for forward Euler (FE) and symplectic Euler (SE) are of order $\mathcal{O}(h)$, while the error for the explicit fourth-order symplectic Euler method

(SE4) and the explicit fourth-order Runge-Kutta method (RK4) are of order $\mathcal{O}(h^4)$. The backward Euler method is not included in the error comparison, because the results coincide with the results for the forward Euler method. Remarkably, the error for the fourth-order Gauss-Legendre (GL4) method only increases as h decreases, due to the increasing rounding error. For SE4, rounding errors start to be significant at $h \approx 0.0008$, while for RK4 this happens at $h \approx 0.003$. Those values of h can be considered as most optimal step-sizes for these methods, because they give the smallest error. We can conclude that the GL4 method performs best with a small step-size.

However, it should be noted that this error comparison is only representative for simulations where rays start exactly on the edge, like in scenario A. A similar error comparison for rays as in scenario B is given in Figure 5.10. Here, $x_0 = -1$, such that the ray starts outside the lens. The Figure shows that all methods are of order $\mathcal{O}(h)$. This is because the error due to *jumping* into the lens at a point instead of starting exactly on the edge of the lens dominates the error due to the method. This makes the GL4 method much less preferable, especially since it is a very expensive method in terms of computational run-time. Taking a faster method like symplectic Euler (SE) with a smaller step-size would therefore make more sense here. However, what would make even more sense is to let the ray start on the edge of the lens to get errors as in Figure 5.9.

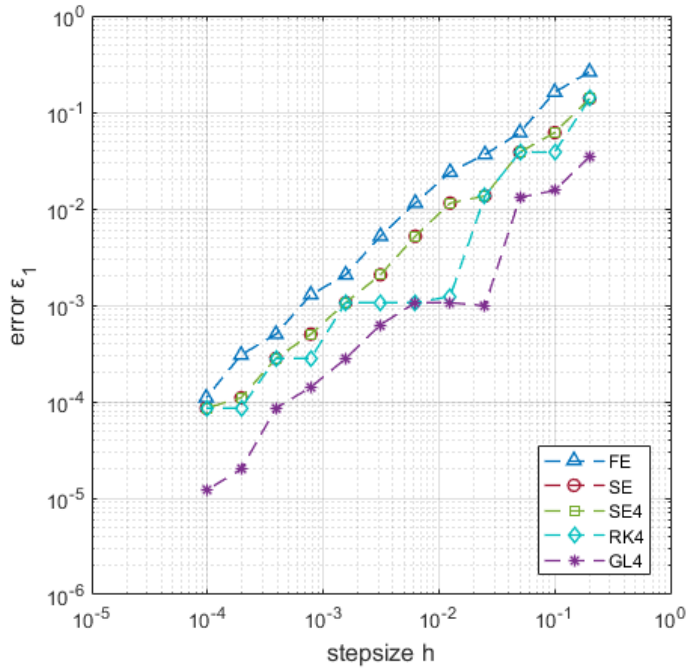

Figure 5.10: Error comparison for a ray starting outside the Luneburg lens.

Another point of discussion is that the error ε_1 does not consider errors outside the lens. Using the current comparison it is misleading to think that the best method is GL4 with a big step-size h. An error comparison for the error in the direction vector outside the lens could be performed to investigate this. Also the error in the momentum vector is not considered, which also could be investigated.

Cylindrical GRIN lens

Next, we consider the cylindrical GRIN lens. For the analytical solution, we consider a ray on the edge and parallel to the z-axis. The analytical solution for this ray is given by [10]

$$y = y_0 \cos\left(\frac{2\pi}{\Lambda} z\right), \tag{5.10}$$

where period Λ is given by equation (5.6). An exact ray is shown in Figure 5.11.

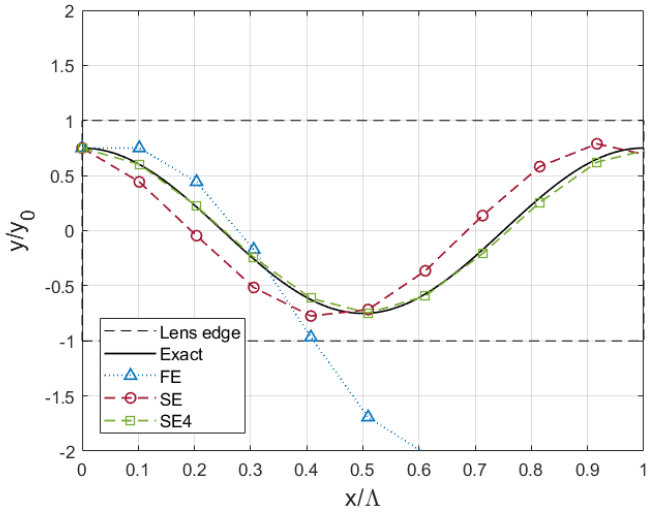

Figure 5.11: Several numerical methods and the exact solution for the cylindrical GRIN lens. $h = 1$, $y_0 = 0.75$, $A = 0.20$, $n_1 = 1.6$, $Z = \Lambda$ and $R = 1$.

For this lens we compare the error ε_1 by using the exact ray solution $y = y(z)$, given by (5.10). The results for a ray as in Figure 5.11 are given in Figure 5.12.

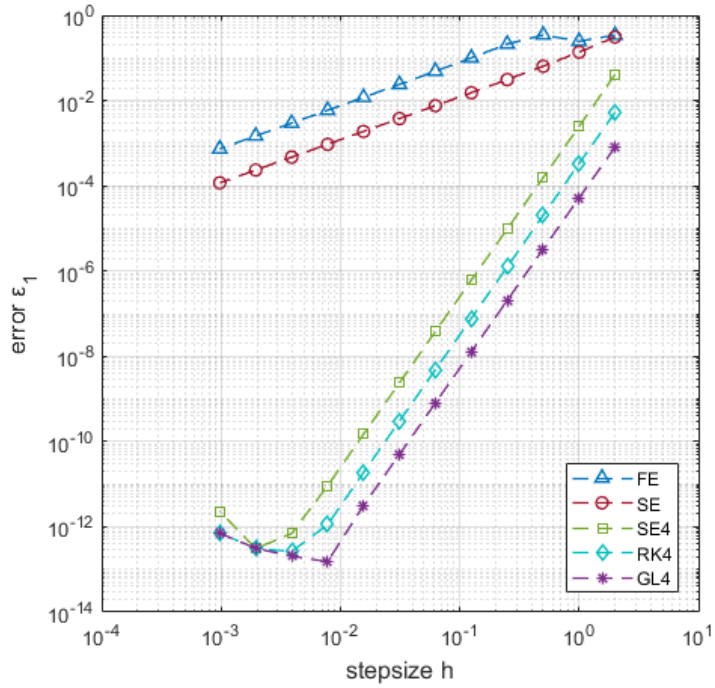

Figure 5.12: Error comparison for the cylindrical GRIN lens.

Figure 5.12 confirms that the error for FE and SE is of order $\mathcal{O}(h)$, while the error for SE4 and RK4 is of order $\mathcal{O}(h^4)$. A different result is that the error for GL4 in this case is of order $\mathcal{O}(h^4)$. If we compare Figure 5.12 with Figure 5.9, we conclude that the symplectic methods, i.e. SE and SE4, perform better for the cylindrical GRIN lens.

5.3 Hamiltonian comparison

The numerical error in the Hamiltonian can be given by

$$\varepsilon_2 = \max |\mathcal{H}_i|, \tag{5.11}$$

for all i such that the corresponding coordinate (x_i, y_i) is inside the lens. The results for a ray in the Luneburg lens as in Figure 5.8 are given in Figure 5.13. For a similar situation in the Maxwell fish-eye lens the results are shown in Figure 5.14. The results for a ray in the cylindrical GRIN lens as in Figure 5.11 are given in Figure 5.15.

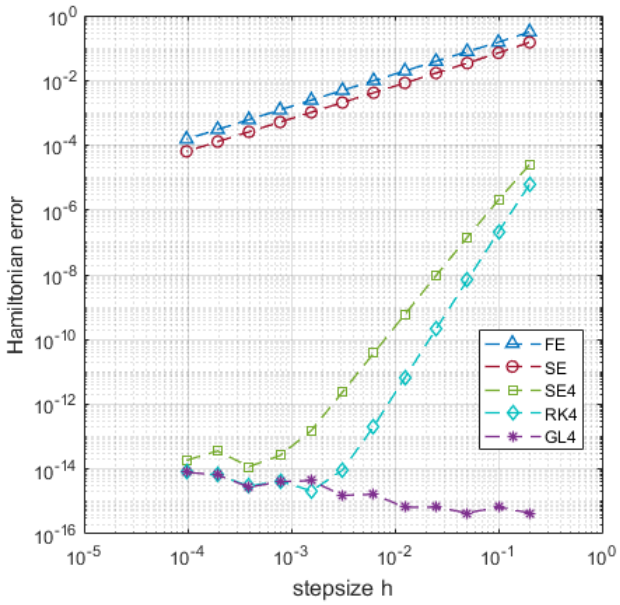

Figure 5.13: Hamiltonian comparison for the Luneburg lens

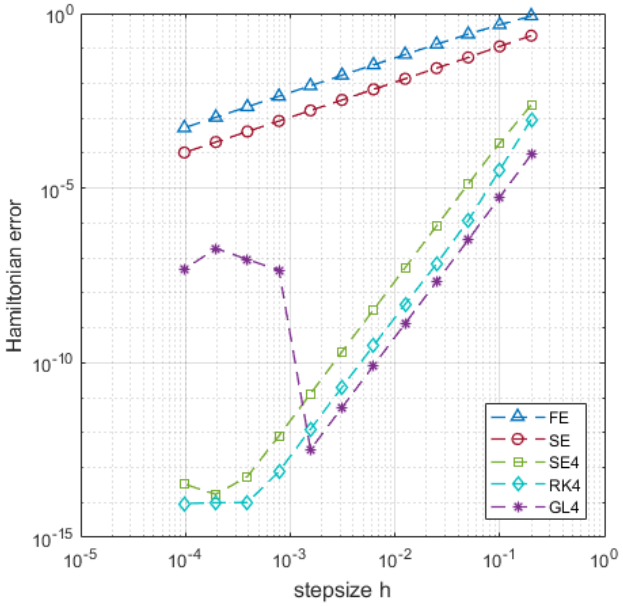

Figure 5.14: Hamiltonian comparison for the Maxwell fish-eye lens

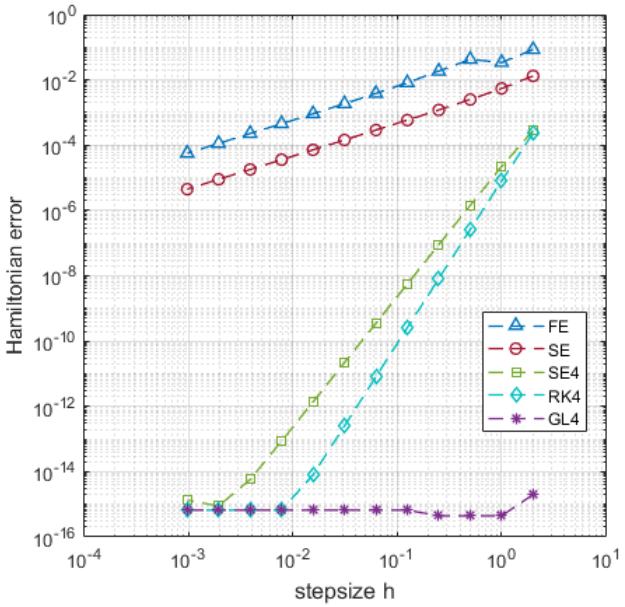

Figure 5.15: Hamiltonian comparison for the cylindrical GRIN lens

Figures 5.13 and 5.15 show similar results, while Figure 5.14 shows a different behaviour for the GL4 method. However, conserving the Hamiltonian does not mean that the numerical solution has a smaller error with the exact solution.

Conclusion

In this report, we have been able to properly define rays and wavefronts in terms of mathematical objects. On the one hand, we have wavefronts, which are surfaces $\psi =$ constant. On the other hand, we have characteristics of the eikonal equation, which coincide with the rays. These characteristics can be obtained by converting the eikonal equation, a nonlinear first-order PDE, into a system of ODEs using the method of characteristics. A summary of the characteristic systems is given in overview 1.4. The system of ODEs can also be written as a Hamiltonian system with a separable Hamiltonian (2.3). All these results can also be obtained in terms of polar coordinates.

After that, we were able to introduce various time integration methods. We covered forward Euler, backward Euler, symplectic Euler, fourth-order symplectic Euler, explicit 4-stage Runge Kutta and fourth-order Gauss-Legendre. Most of these methods are rather standard, except for the fourth-order symplectic Euler scheme. This method uses Runge-Kutta stages where some coefficients are relatively large and negative. Furthermore, we described the following lenses: the Luneburg lens, the Maxwell fish-eye lens, the cylindrical GRIN lens and even a variant of the latter called the cylindrical hyperbolic-secant GRIN lens. After that, numerical results were presented, containing the simulation of rays and wavefronts for the various lenses. In the error comparison, we used two errors ε_1 and ε_2. Here, ε_1 was defined as the maximum vertical distance with respect to the exact solution and ε_2 was defined as the maximum error in the Hamiltonian. The errors were determined for several step sizes h for the spherical Luneburg lens and the cylindrical GRIN lens. The conclusions are summarized in table 5.1. The table shows the orders of the errors.

Numerical method	**Error** ε_1	**Error** ε_2
Forward Euler	$\mathcal{O}(h)$	$\mathcal{O}(h)$
Backward Euler	$\mathcal{O}(h)$	$\mathcal{O}(h)$
Symplectic Euler	$\mathcal{O}(h)$	$\mathcal{O}(h)$
4^{th}-order symplectic Euler	$\mathcal{O}(h^4)$	$\mathcal{O}(h^4)$
4-stage Runge-Kutta	$\mathcal{O}(h^4)$	$\mathcal{O}(h^4)$
4^{th}-order Gauss-Legendre	$*/\mathcal{O}(h^4)$	$*$

Table 5.1: Summary of the results from the error comparison. * indicates that there is no significant error convergence with respect to h. The error in this case is dominated by the rounding error.

We can conclude that the Hamiltonian enables us to compare methods, without having to know the exact solution, which is often hard to get. Also, within the compared methods,

the Gauss-Legendre method gives the smallest error with the exact solution, and can therefore be considered as the best method for simulating rays and wavefronts. However, we did not perform a running time analysis. So if running time is a constraint for the algorithm, then a different method may be preferred. Also the errors described do not include effects outside the lens. Those errors are especially significant for big step-sizes, which can not be concluded for the Luneburg lens by either error ε_1 or ε_2. Nevertheless, this report gives a foundation on the mathematical model for simulating light within the Geometric Optics model and can be easily extended to any optical lens or gradient-index medium.

References

[1] Mohammad D. Al-Amri, Mohamed M. El-Gomati and M. Suhail Zubairy. *Optics in our time*. Springer International Publishing, Jan. 2016, pp. 1–504. ISBN: 9783319319032. DOI: 10.1007/978-3-319-31903-2.

[2] Arnt Inge Vistnes. *Geometric Optics*. 2018, pp. 371–417. ISBN: 9783319437316. DOI: 10.1007/978-3-319-72314-3{_}12.

[3] John A. Adam. *Rays, Waves, and Scattering*. 2017. ISBN: 9780691148373. DOI: 10.2307/j.ctt1vxm7wt.

[4] Witold A.J. Kosmala. *A Friendly Introduction to Analysis; Single and Multivariable*. 2004, p. 591. ISBN: 0-13-045796-5.

[5] Dmitry S. Kulyabov, Anna V. Korolkova, Tatiana R. Velieva et al. "Numerical analysis of eikonal equation". In: June 2019 (2019), p. 56. ISSN: 16057422. DOI: 10.1117/12.2525142.

[6] Robert A Adams and Christopher Essex. *Calculus : a complete course LK - https://tue.on.worldcat.org/oclc/1039886914*. Engels. Ninth edit. Toronto SE - 1085 pages; 28 cm.: Pearson Canada Inc., 2017. ISBN: 9780134154367 0134154363.

[7] Haruo Yoshida. "Construction of higher order symplectic integrators". In: *Physics Letters A* 150.5-7 (1990), pp. 262–268. ISSN: 03759601. DOI: 10.1016/0375-9601(90)90092-3.

[8] Etienne Forest and Ronald D. Ruth. "Fourth-order symplectic integration". In: *Physica D: Nonlinear Phenomena* 43.1 (May 1990), pp. 105–117. ISSN: 01672789. DOI: 10.1016/0167-2789(90)90019-L.

[9] Christian R. Ocier, Corey A. Richards, Daniel A. Bacon-Brown et al. "Direct laser writing of volumetric gradient index lenses and waveguides". In: *Light: Science and Applications* 9.1 (2020). ISSN: 20477538. DOI: 10.1038/s41377-020-00431-3.

[10] Hiroshi Ohno. "Symplectic ray tracing based on Hamiltonian optics in gradient-index media". In: *Journal of the Optical Society of America A* 37.3 (2020), p. 411. ISSN: 1084-7529. DOI: 10.1364/josaa.378829.

[11] Carlos Gomez-Reino, Maria Victoria Perez and Carmen Bao. *Gradient-Index Optics*. Springer Berlin Heidelberg, 2002. DOI: 10.1007/978-3-662-04741-5.

[12] Jesús Liñares and Carlos Gómez-Reino. "Optical propagator in a graded-index medium with a hyperbolic secant refractive-index profile". In: *Applied Optics* 33.16 (1994), p. 3427. ISSN: 0003-6935. DOI: 10.1364/ao.33.003427.